Overview about rock mechanical lab testing – part II: visualisation and structure analysis

Authors: Prof. Dr. habil. Heinz Konietzky, Dr. Yufeng Zhao (TU Bergakademie Freiberg, Geotechnical Institute) & Dr. Thomas Frühwirt (TU Graz, Institut of Rock Mechanics and Tunneling)

Editor: Prof. Dr.-Ing. habil. Heinz Konietzky Layout: Gunther Lüttschwager, Angela Griebsch
TU Bergakademie Freiberg, Institut für Geotechnik, Gustav-Zeuner-Straße 1, 09599 Freiberg • sekr_fm@ifgt.tu-freiberg.de

1 Introduction

Detailed rock mechanical investigations do not only include the measurement of stress-strain relations and ultimate loads, but need also an in-depth going analysis of the structure of the material. This includes for instance:

- Analysis of grain and pore structure (size, shape, distribution etc.)
- Mineralogical composition
- Fracture pattern
- Micromechanical damage analysis (micro cracks)
- Surface roughness of samples or joints
- Joint and fracture detection
- Microstratigraphy

For rock mechanical tasks the following types of visualization are common:

- Laser-Scanning
- Tomography (CT)
- Core scanner
- High speed camera
- Photo-Documentation
- Microscopy

All these techniques are non-destructive. Digital images can be produced and used for documentation. Some of them can be used during the rock mechanical testing, so that structural changes (e.g. damage pattern, fracture development etc.) can be observed and correlated to the loading stage.

2 Photo documentation

A detailed photo documentation is a necessary component of any lab report and should allow to get an impression about the tested rock type, size and shape of samples as well as fracture pattern after testing (fig. 1). Detailed photos allow to evaluate grain size, grain shape and mineralogical content (fig. 2). All samples should be named, so that all data and information can be assigned.

Fig. 1: Granite samples before (top left) and after testing (else) (RML 2016)

Fig. 2: Granite sample before testing (RML 2016)

3 Core scanner

Core scanners use line-scan cameras with white or ultraviolet light to analyse drill cores. They deliver 3D surface images of cores for digital documentation and analysis, especially for structural and petrological reasons. Typically, the use of core scanners comprises two steps: (i) scanning and storage of digital images (fig. 3) and (ii) detailed software based analysis of structure and petrological composition (e.g. fracture and bedding detection and orientation, grain size analysis, mineralogical composition analysis, RQD value determination etc. (fig. 4).

Typical parameters are:

- Resolution up to about 50 pixel/mm (> 1000 dpi)
- Scan speed: 0.05 m/s

Fig. 3: Core scan device in operation (DMT: company material)

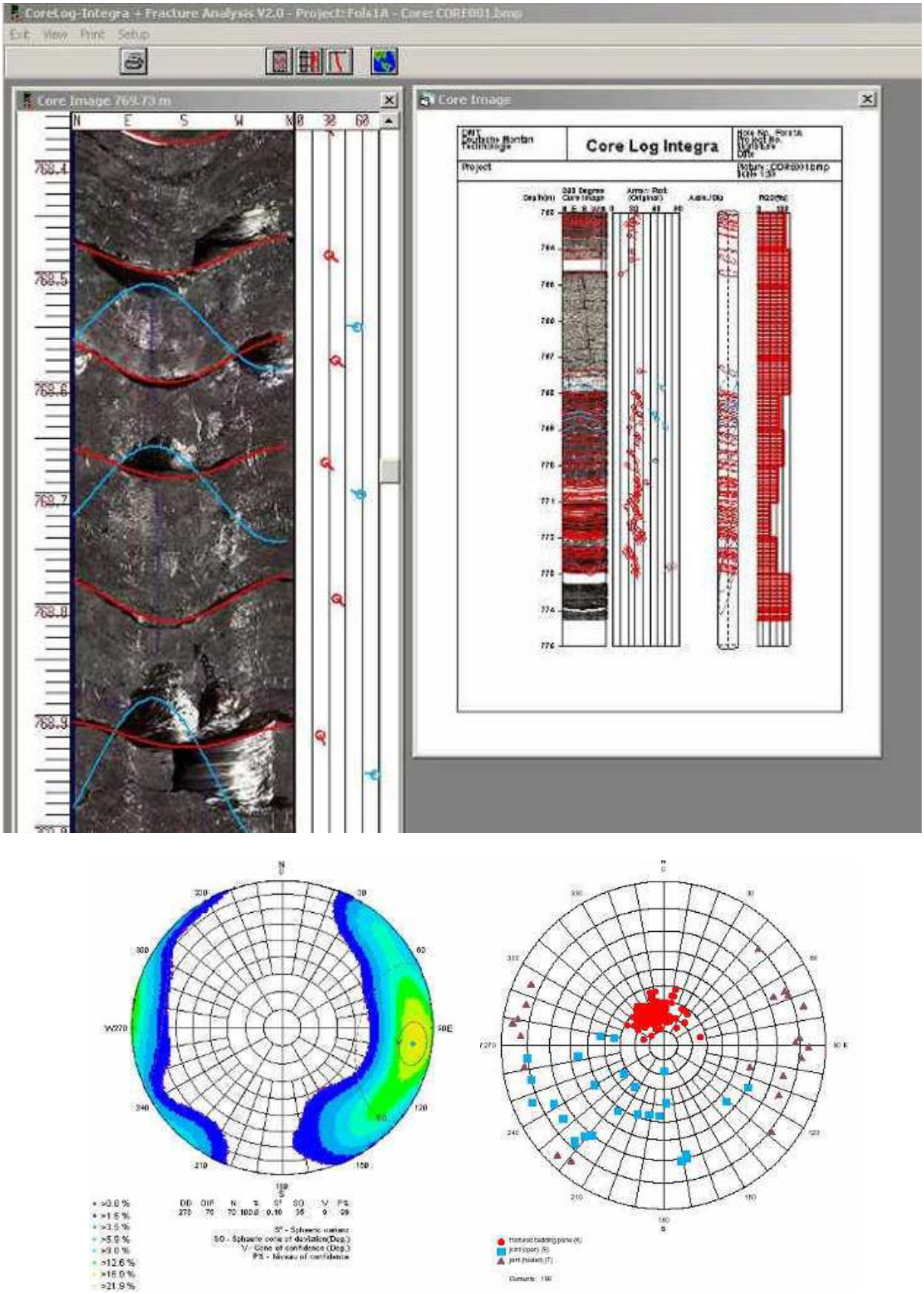

Fig. 4: Core with marked fractures and corresponding software based analysis results (DMT: company material)

4 Microscopy

Microscopy can be subdivided into three categories:

- Optical (light) microscopy: resolution of up to about 1 µm
- Electron microscopy: resolution of up to about 1 nm
- Scanning probe microscopy: resolution of up to about 1 nm

Electron microscopy comprises **T**ransmission **E**lectron **M**icroscopy (TEM) and **S**canning **E**lectron **M**icroscopy (SEM). These techniques use electron beams. Scanning probe microscopes scan the surface of samples with the help of a probe tip and the interaction is used to measure fine surface shapes or properties.

Tab. 1: Classification of optical microscopes (Keyence 2016)

Binocular stereoscopic microscope	A microscope that allows easy observation of 3D objects at low magnification.
Bright field microscope	A typical microscope that uses transmitted light to observe targets at high magnification.
Polarizing microscope	A microscope that uses different light transmission characteristics of materials, such as crystalline structures, to produce an image.
Phase contrast microscope	A microscope that visualizes minute surface irregularities by using light interference. It is commonly used to observe living cells without staining them.
Differential interference contrast microscope	This microscope, similar to the phase contrast, is used to observe minute surface irregularities but at a higher resolution. However, the use of polarized light limits the variety of observable specimen containers.
Fluorescence microscope	A biological microscope that observes fluorescence emitted by samples by using special light sources such as mercury lamps. When combined with additional equipment, bright field microscopes can also perform fluorescence imaging.
Total internal reflection fluorescence microscope	A fluorescence microscope that uses an evanescent wave to only illuminate near the surface of a specimen. The region that is viewed is generally very thin compared to conventional microscopes. Observation is possible in molecular units due to reduced background light.
Laser microscope (Laser scanning confocal microscope)	This microscope uses laser beams for clear observation of thick samples with different focal distances.
Multiphoton excitation microscope	The use of multiple excitation lasers reduces damage to cells and allows high-resolution observation of deep areas. This type of microscope is used to observe nerve cells and blood flow in the brain.
Structured illumination microscope	A high-resolution microscope with advanced technology to overcome limited resolution found in optical microscopes that is caused by the diffraction of light.

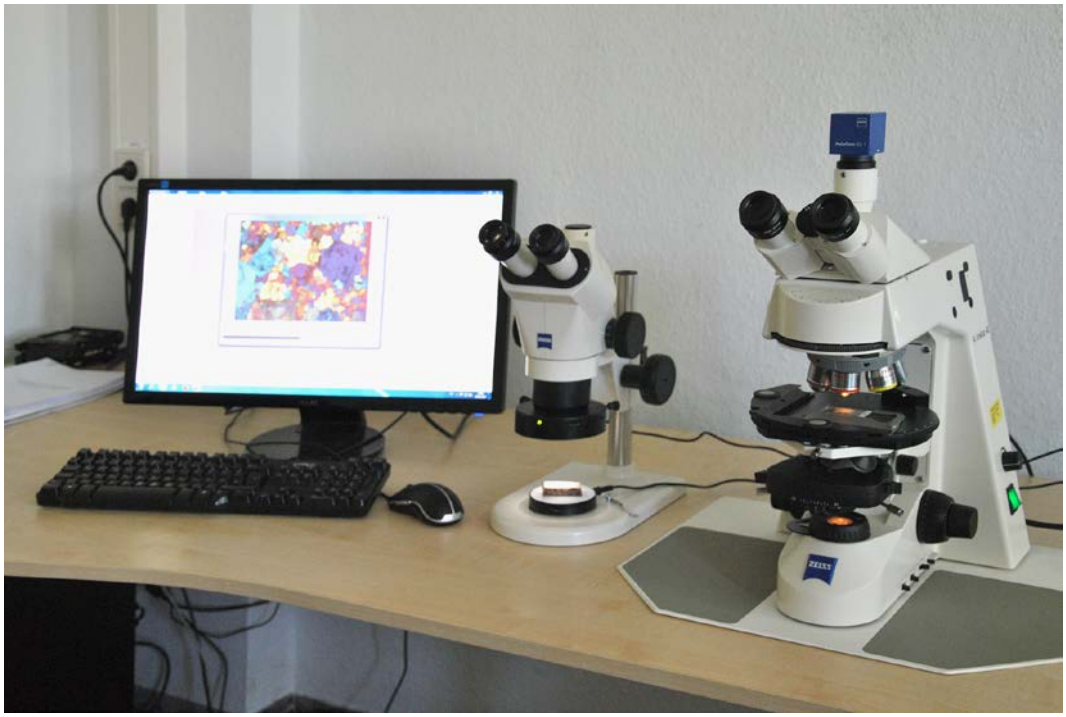

Fig. 5: Polarising microscope Axioscop 40 with digital camera (right) and binocular stereo microscope Stemi 2000-C (left) (RML 2016).

With a polarizing microscope (fig. 5) it is possible to investigate the mineralogical composition and fabric of rocks on thin sections with a typical magnification of 200, which can be extended by additional objectives to obtain larger magnification. Such a microscope is often equipped with a digital camera, which is connected to an image analysis software. It is possible to gain a live image and to investigate the phenomena on it. Live images can be saved to scaled microphotographs for later measurements such as the grain or pore shape and size analysis or quantification of the mineralogical composition (fig. 6).

With a typical stereo microscope, like Stemi 2000-C by Carl Zeiss, it is possible to analyse particles or the surface of objects with a maximum magnification of factor 100. With a polarising microscope like the Axioscop 40, it is possible to gain live images and save them as scaled micro photographs for later analysis. For the image analysis of greyscale micro photographs special software packages like “Image SXM” or “ImageJ” can be used. They provide numerous options for image processing and analysis.

More precise pictures, especially with options to measure surface profiles, can be obtained by **S**canning **E**lectron **M**icroscopy (SEM), as illustrated in fig. 7. Optical 3D-microscopy allows to measure 3-dimensional structures (fig. 8).

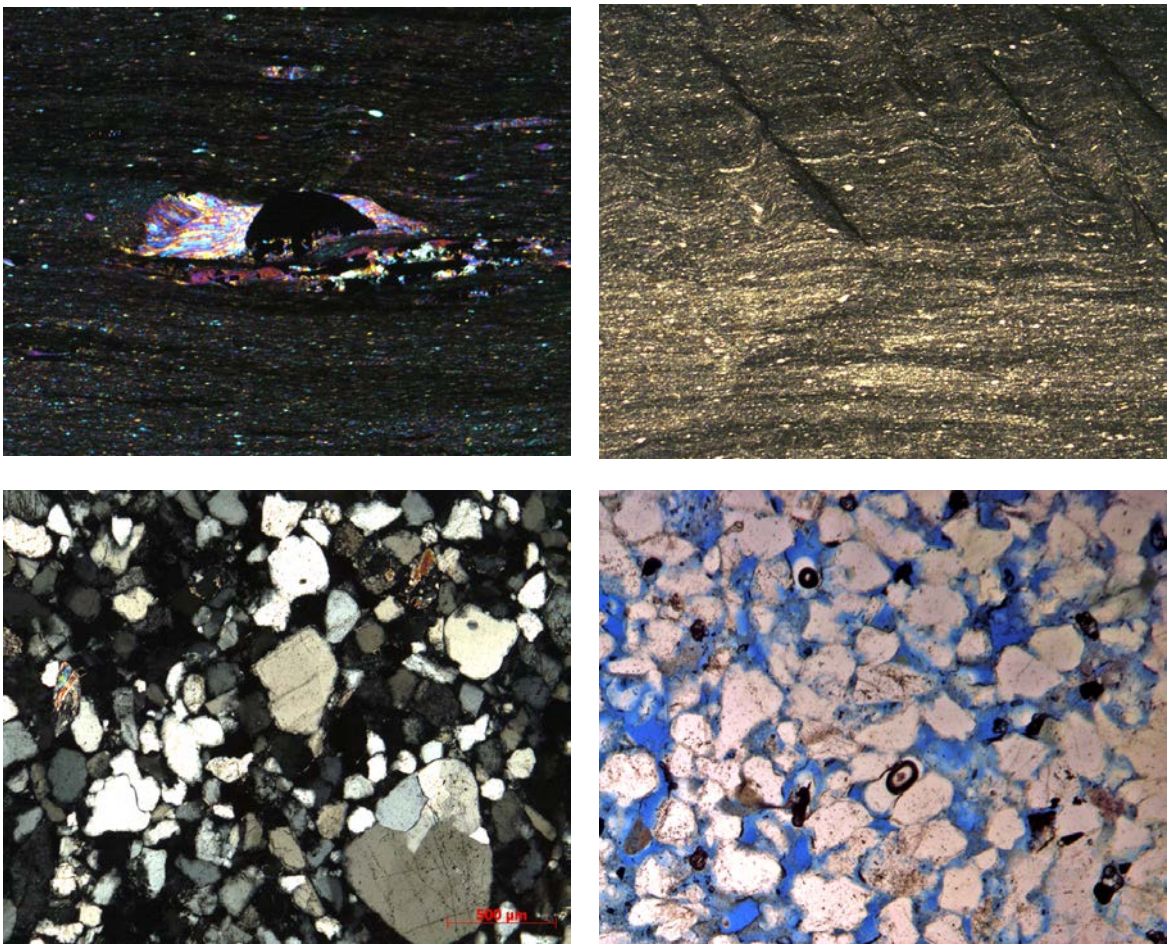

Fig. 6: Micro photographs gained by the Axioscop 40. Upper left: Pressure shadows around an opaque mineral in a slate as a result of pressure-solution processes. Upper right: Crenulation foliation which overprints the horizontally orientated fracture cleavage within a slate. Note that the crenulation foliation disappears within the more competent layer. Lower left: Quartzitic sandstone used for the buildings of the Cistercian monastery in Osek in Northern Bohemia. Lower right: The blue resign shows the pore space of the Cotta sandstone in Southeast Germany (except for lower left: width of view = 1.3 mm) (RML 2016).

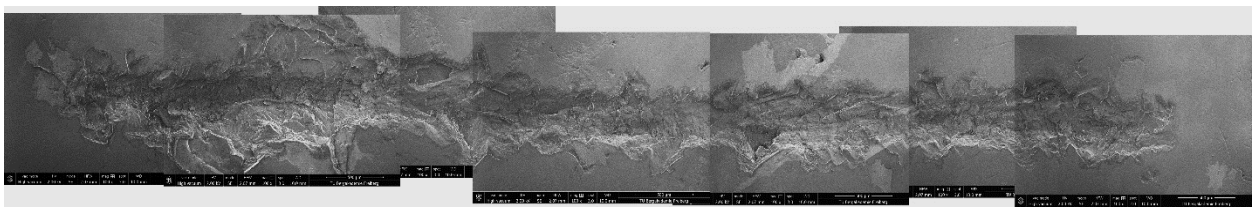

Fig. 7: Scanning electron microscopic image of Cherchar scratch test (magnification: 1:100)

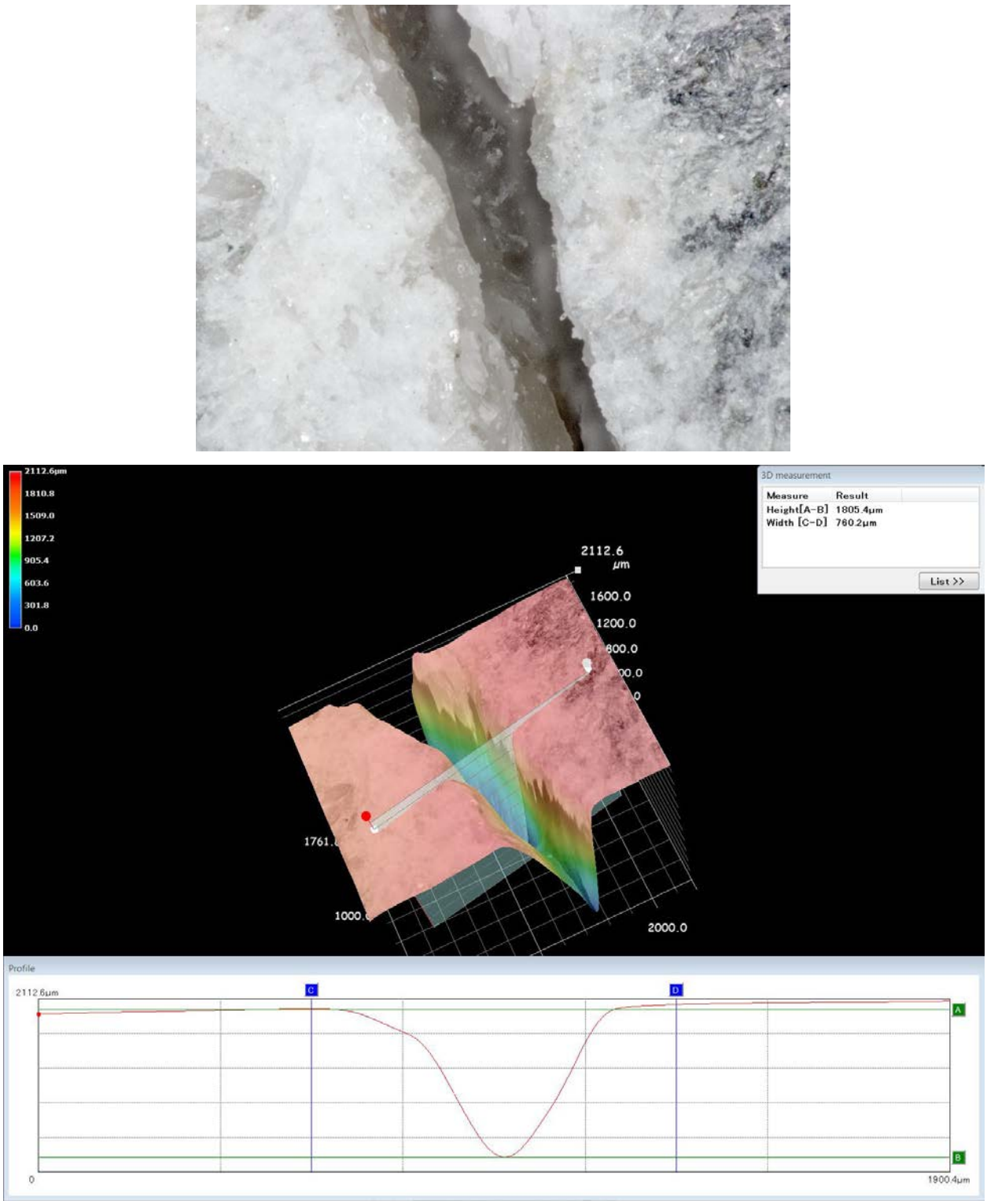

Fig. 8: Microscopic view of a microscopic crack in granite (top) and optical 3D-measurement with Keyence microscope (bottom) of crack (depth of crack: 1800 – 2000 µm, opening: 500 – 700µm) (RML 2016)

5 X-ray tomography

Tomography is the study of the three dimensional structure of an object by slicing it into thin sections. X-ray transmission technology as a special kind of tomography allows to analyse the internal structure of rocks (pore structure, fractures, grain shape and size etc.) without disturbing the sample (non-destructive testing method). **C**omputer **T**omography (CT) is a standard tool in medicine, but is nowadays also widely used in other fields like material sciences and also rock mechanics. The transmission CT consists of two parts: an X-ray source and an X-ray detector (fig. 9). Between these two components the sample is placed on a rotational platform (fig. 10). The closer the sample is placed to the source, the higher the magnification is. Resolution depends on several factors like distance between source and sample, focal spot size, pixel size of detector, X-ray scattering etc. (tab. 2). The typical power of such systems is between 250 and 1000 keV. Higher power allows the investigation of bigger samples. Post-processing of image data by special software packages is a complex matter and under permanent development, but leads to significant improvement of images (figures 11 and 12).

Tab. 2: Typical parameters for different CT tools

Parameter	Medical-CT	Micro-CT	Nano-CT
Typical sample dimension / mm	1000	100	1
Typical spatial resolution / µm	250	5	0.05

Fig. 9: CT device XT-H-450 (power: 450 keV) (Inst. Geonics, Czech Republic)

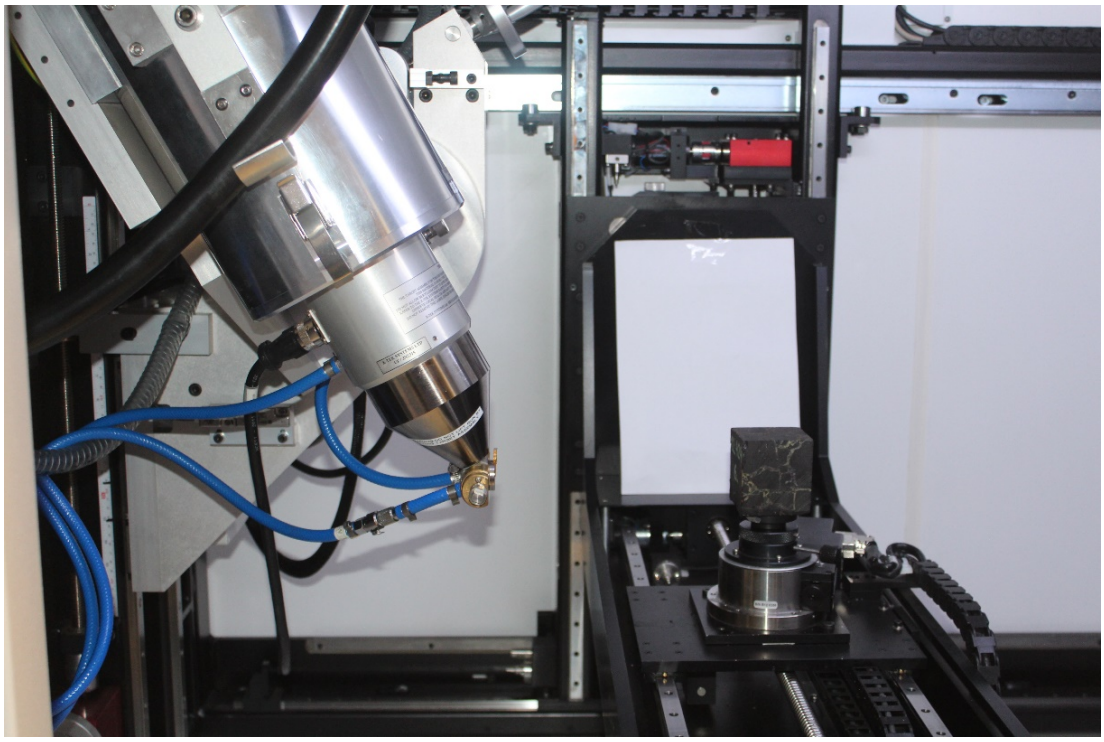

Fig. 10: X-ray source and cubic sample (Inst. of Geonics, Czech Republic)

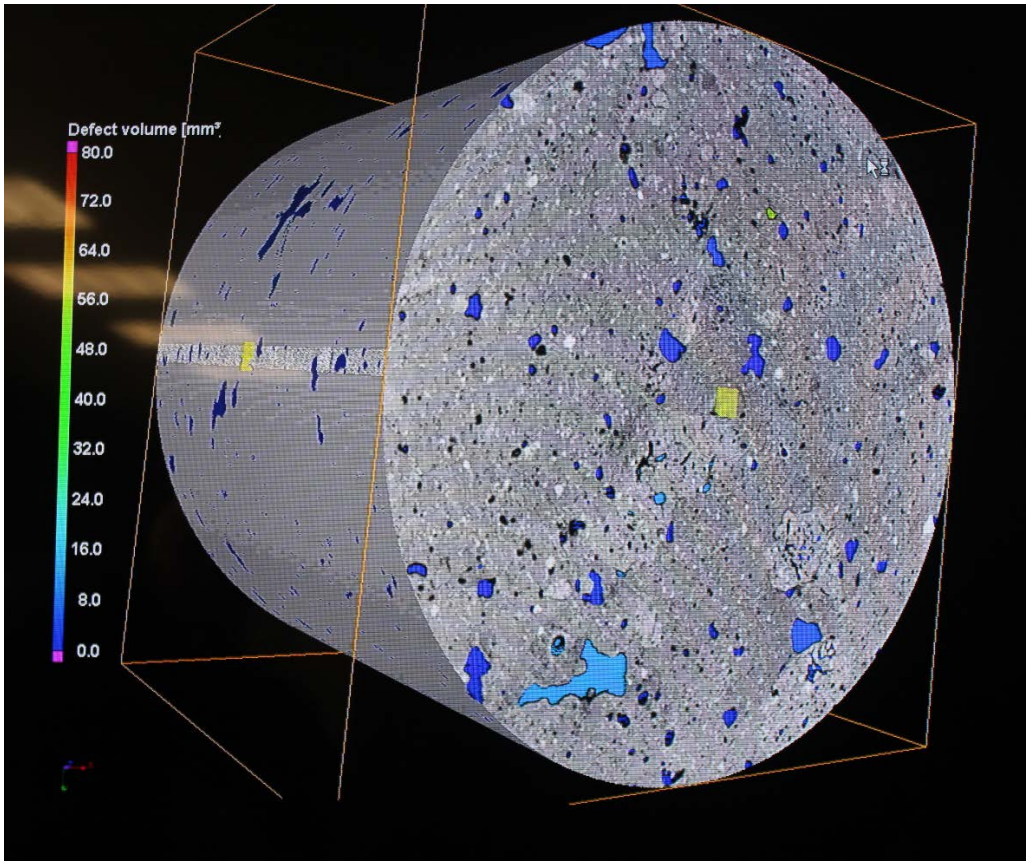

Fig. 11: Investigated rock sample with 3D structures (Inst. of Geonics, Czech Republic)

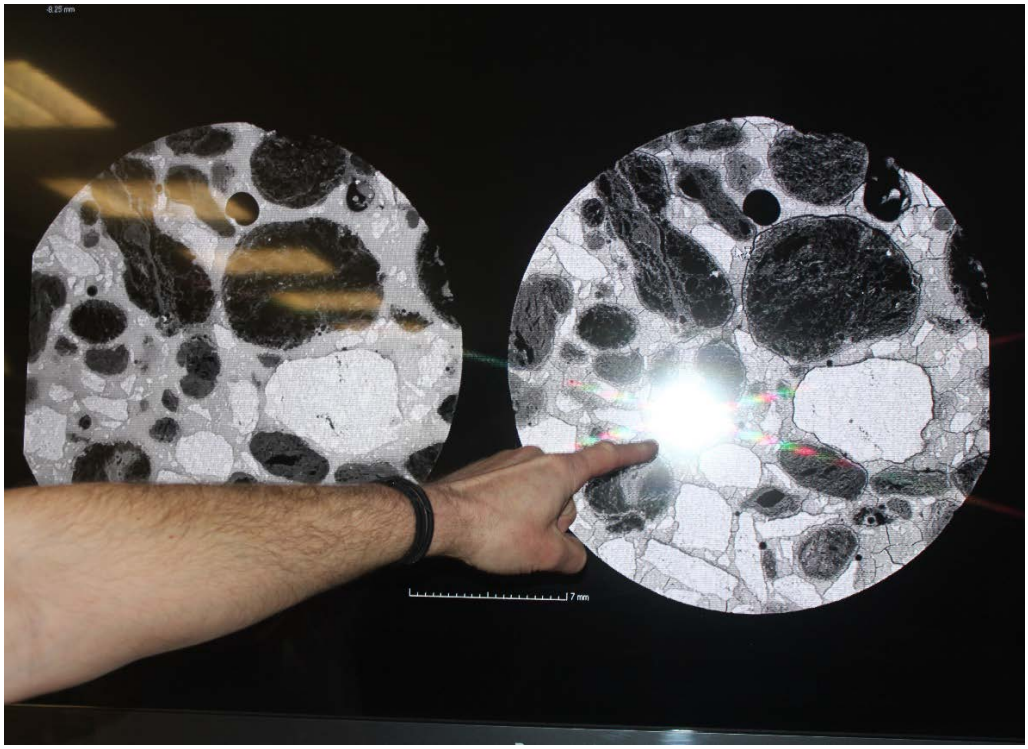

Fig. 12: Investigated rock sample with 2D structures (Inst. of Geonics, Czech Republic)

Example (Kaczmarek et al., 2017)

An ACTIS-225FFI micro-xCT scanner was used to scan coal specimen as shown in fig. 13a. The minimum resolution of the scanner is 10 µm for a cubic sample size of 4.8 mm. Under the applied conditions of the conducted experiments (180 kV, 200 µA at a raster of 750 × 750 pixels) the resolution is approximately 50 × 50 µm^2. The scan time is 9 seconds per slice. Both, slice thickness and slice spacing are 0.05 mm. Fig. 13 shows the layout of micro focus xCT device and the scanned slices of the specimen.

A uniaxial rock testing system was added to the scanner, so that damage evolution can be monitored during the loading. Intact coal specimen was scanned before the test. The load was applied in steps of 500 N i.e., 500 N, 1000 N, 1500 N etc. At each load level CT scanning was performed. The obtained CT scanning images of a coal specimen are shown in fig. 13c which provide 2D structural information of the cross-section. Around 1000 images from each stage of the uniaxial compression test were obtained and used to reconstruct the 3D structure of the sample using a digital image processing software. First the level and exposure were adjusted automatically to illustrate the basic information, then the input level curves were manually adjusted to achieve better visual qualities.

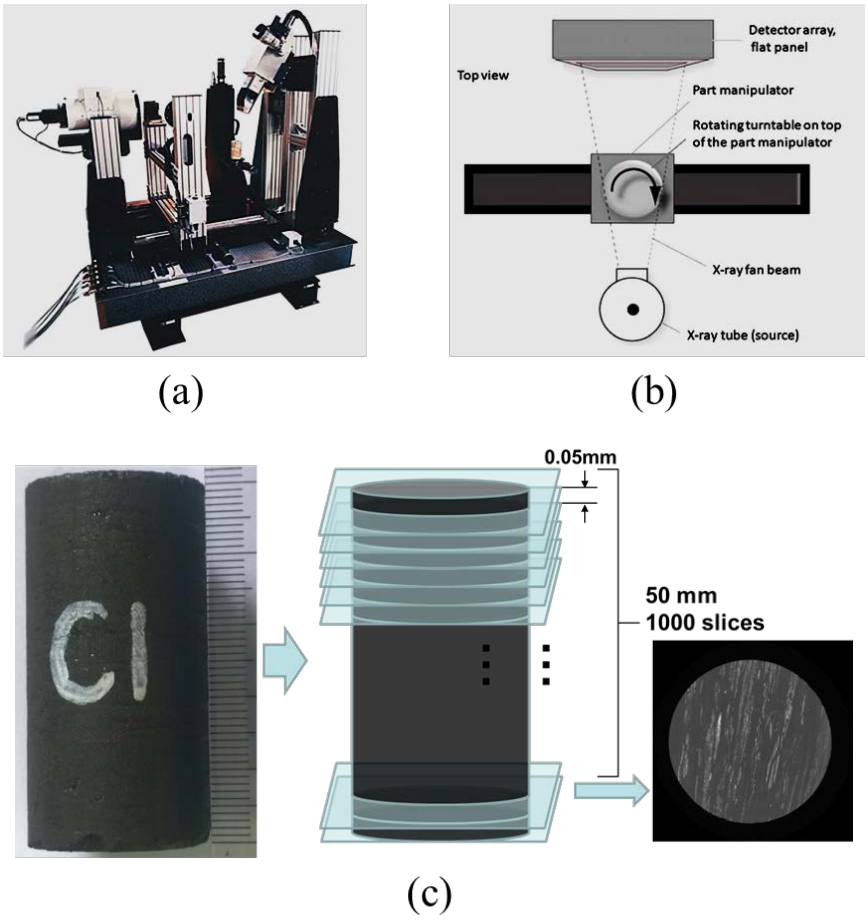

Fig. 13: Micro-xCT scanner associated with rock testing system. (a) Micro-xCT scanning device. (b) Top view of the schematic layout of the scanner. (c) Specimen dimensions and scan slice spacing.

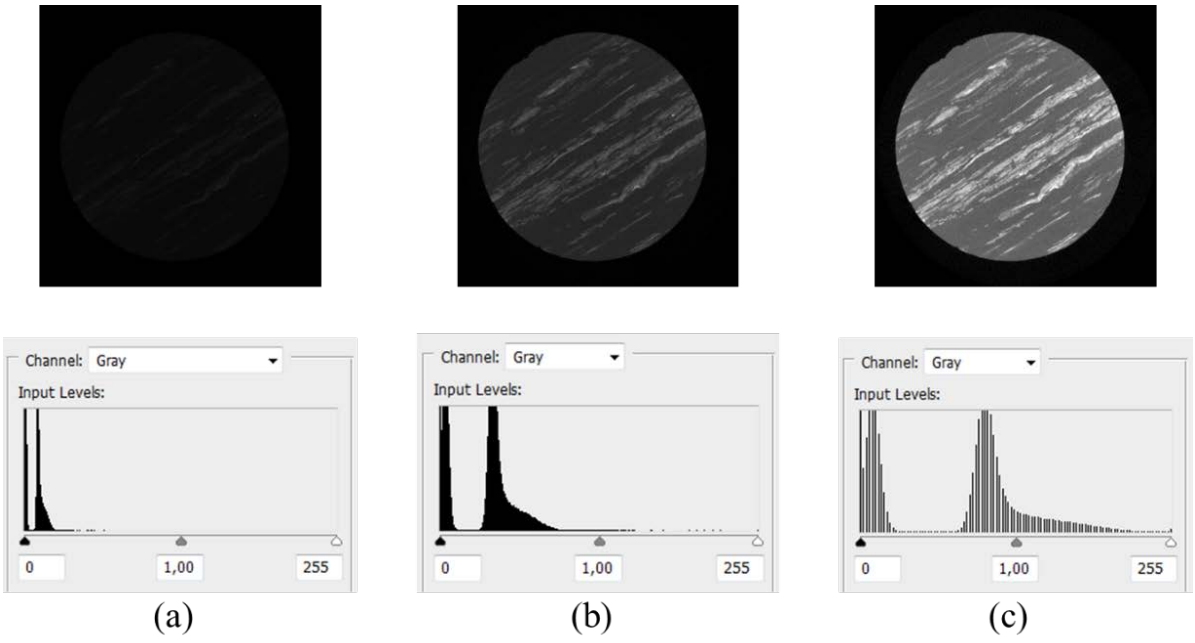

Fig. 14: Input level curves at different phases: (a) raw image, (b) automatically adjusted image and (c) manually adjusted image

In a next step the noise - caused by the unstable exposure during the scanning - was minimized by a special software. Then, the resolution was reduced by threshold segmentation to simplify the calculation procedure (fig. 15). According to the different grayscale values, the characteristics of the coal matrix and mineral inclusion can be obtained. Using this information, one can adjust the grayscale values to the mineral components and defects. As shown in fig. 15b, the black areas represent the background and the voids; the gray area represents the coal matrix; and the white area represents the mineral content.

A total of 1010 scanned X-ray images (fig. 16a) of the coal specimen were stacked using the Mimics software and a 3D specimen with the microstructural information was reconstructed as shown in fig. 16b and 16c. Fig. 17 shows the complete stress-strain curve of the uniaxial compression test together with some reconstructed samples indicating the internal structure and damage.

The geometries of the coal matrix and mineral inclusions were exported from the Mimics software into a STL format, which can be used to set-up numerical models with detailed micromechanical structure. Exemplary, fig. 18 shows micro-mechanical models based on the above mentioned CT image processing using PFC^{2D} and PFC^{3D} (both are particle based codes) as well as FLAC^{3D} (classical mesh-based code).

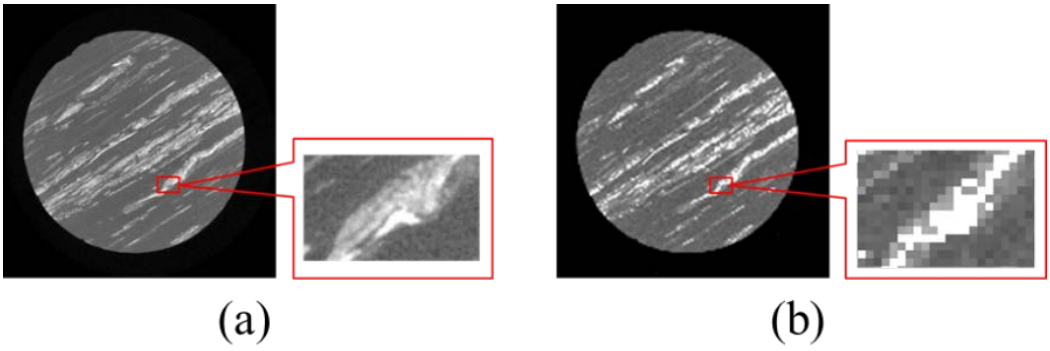

Fig. 15: Resolution reduction and grayscale value segmentation

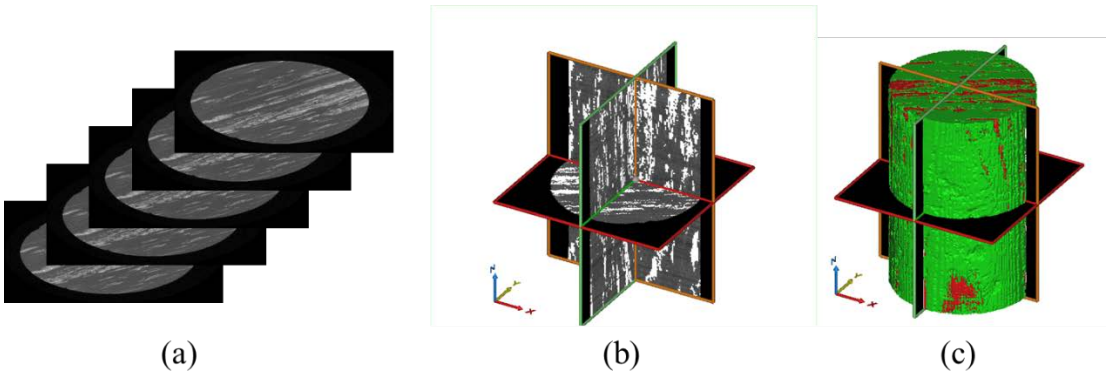

Fig. 16: 3D Model reconstruction based on stacked from 2D images

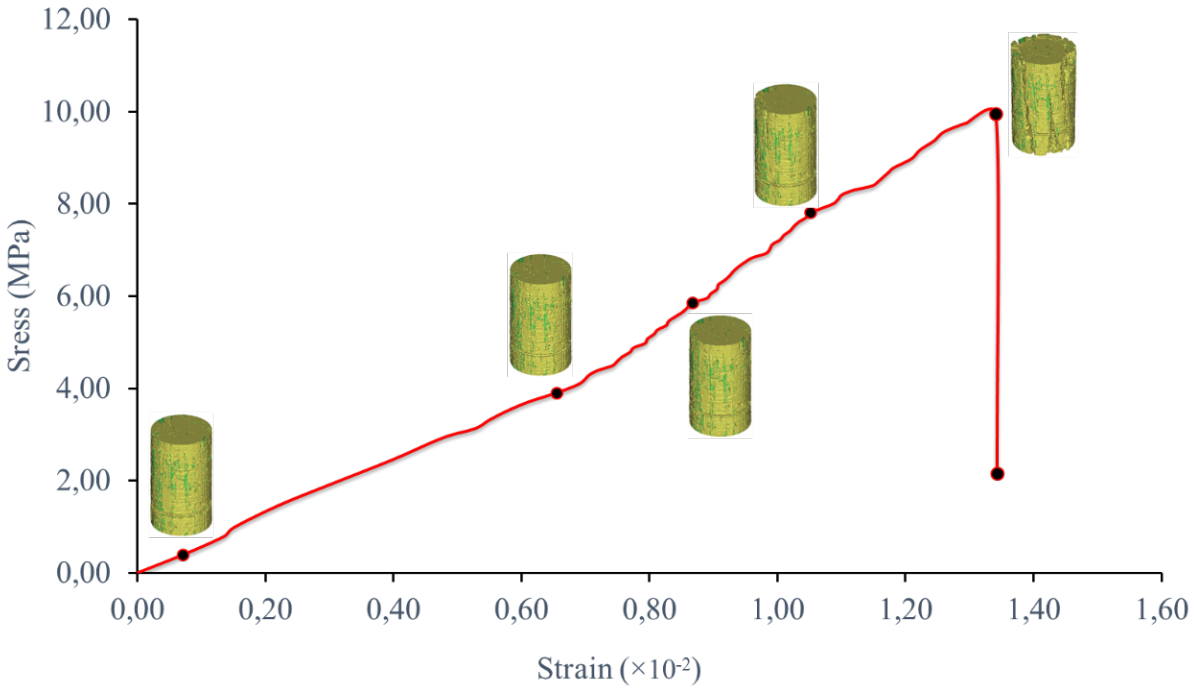

Fig. 17: Stress-strain curve of specimen and reconstructed samples for selected loading stages

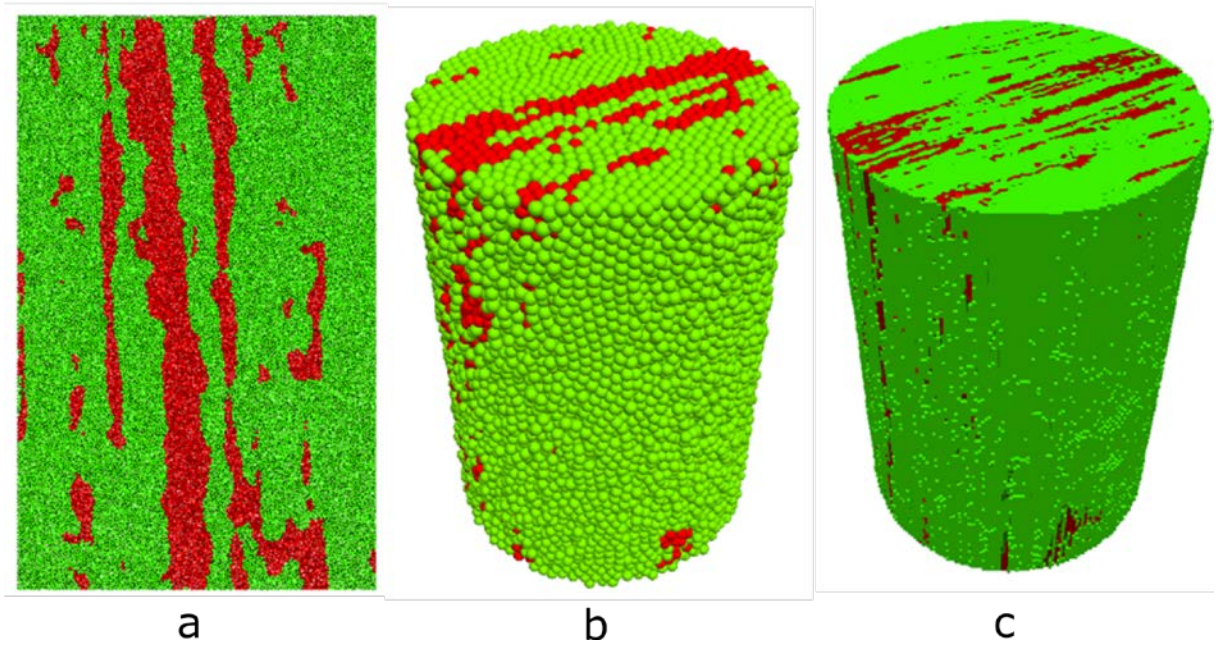

Fig. 18: Numerical model reconstruction in different numerical software (a: PFC^{2D}, b: PFC^{3D}, Flac^{3D})

6 High-speed cameras

Several phenomena like brittle fracturing are characterized by extremely high speed. To get detailed information about the process digital high-speed cameras also called slow-motion cameras (> 250 frames per second) are used (fig. 19). Typically several thousand to several hundred thousand frames per second are used. Increasing frame rate leads to reduced resolution (reduced number of pixels).

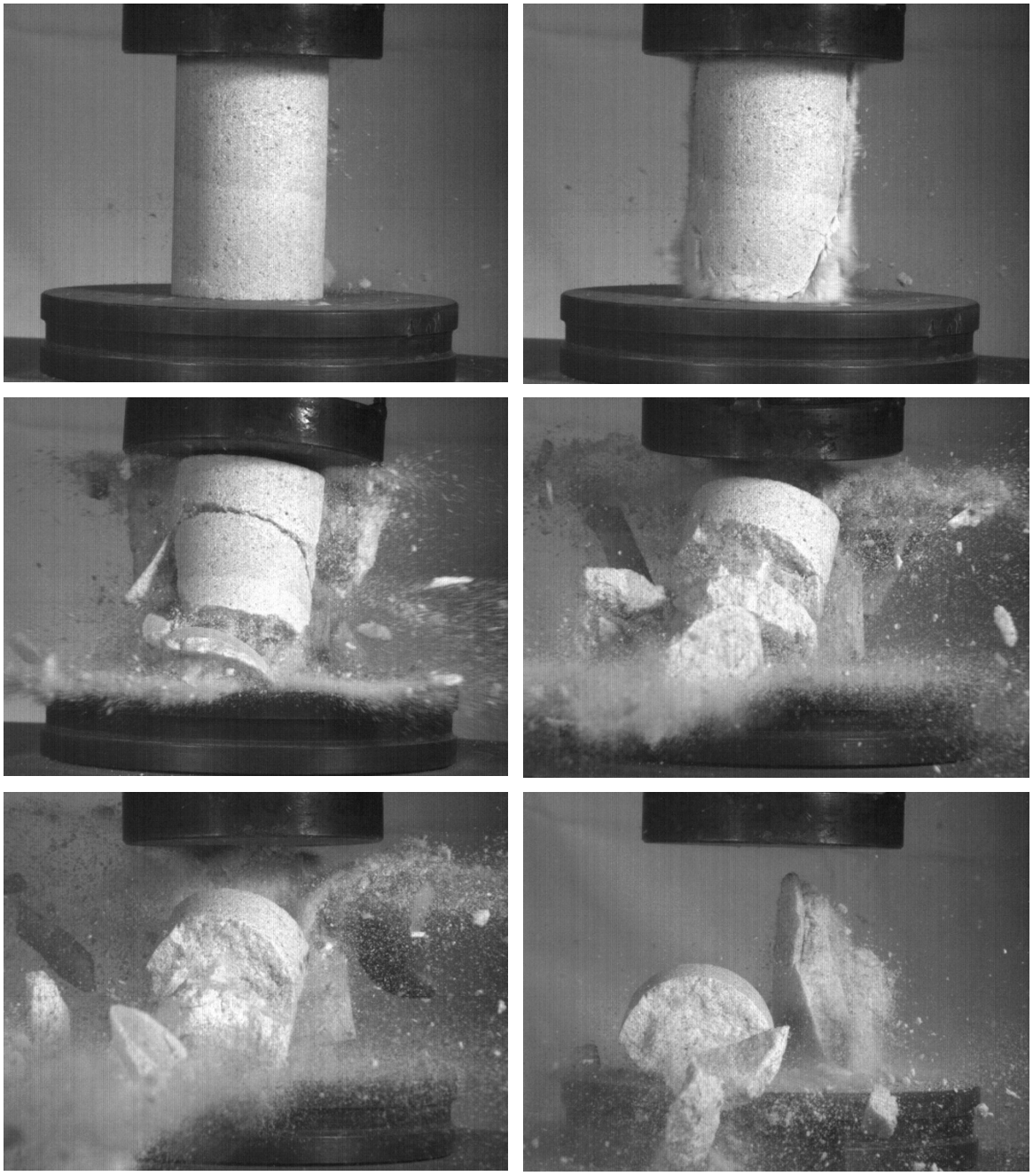

Fig. 19: High-speed camera images from uniaxial compression test (RML 2016)

7 Laser scanner

Laser scanning is the controlled steering of laser beams followed by a distance measurement at every pointing direction. Typical resolution for lab equipment is a few micrometres. Short range scanners used in labs scan small individual objects of up to about 1 m in extension. Most short range scanners operate on the principle of triangulation where a laser is emitted and returned to a specific location on a CCD array of an inboard camera. Triangulation systems typically have an operating range of 0.5 m – 2 m. Besides the classical line by line scanning technology new technologies like full-field triangulation is used. The basic principle of operation for the zSnapper scanners (fig. 20) is the phase encoded photogrammetry which is a version of full-field triangulation and represents technology advancement for the well-known and precise white light scanners. Exemplarily a scanned surface is shown in fig.21.

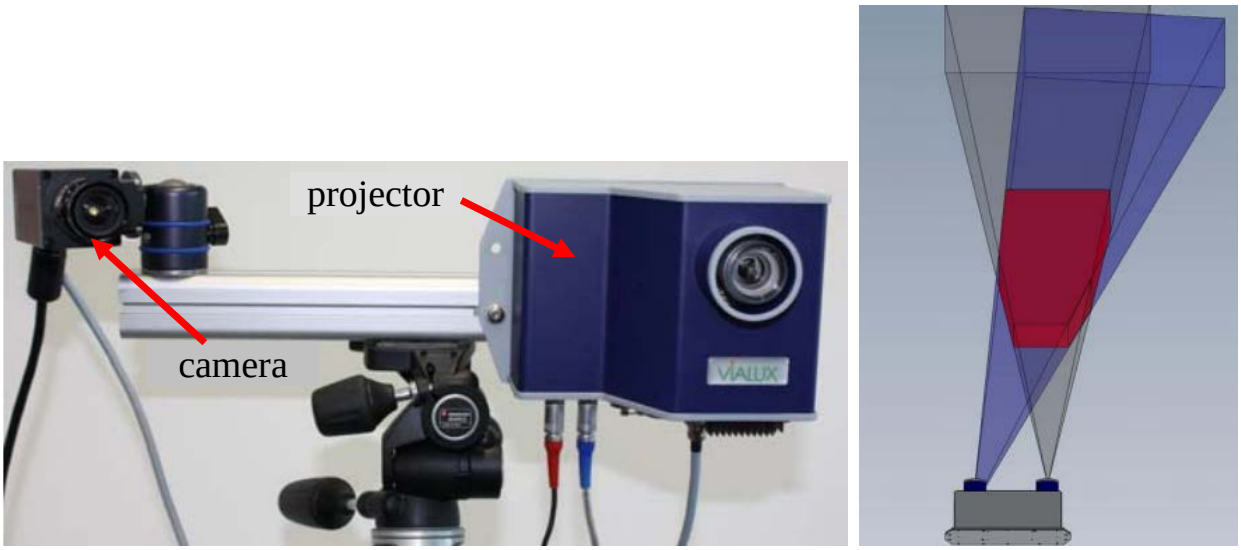

Fig. 20: zSnapper (Vialux 2010) scanning device (accuracy about 20 µm, resolution up to 4.200.000 pixels, field of views up to 1 m, scanning time between 20 and 200 ms), (RML 2016).

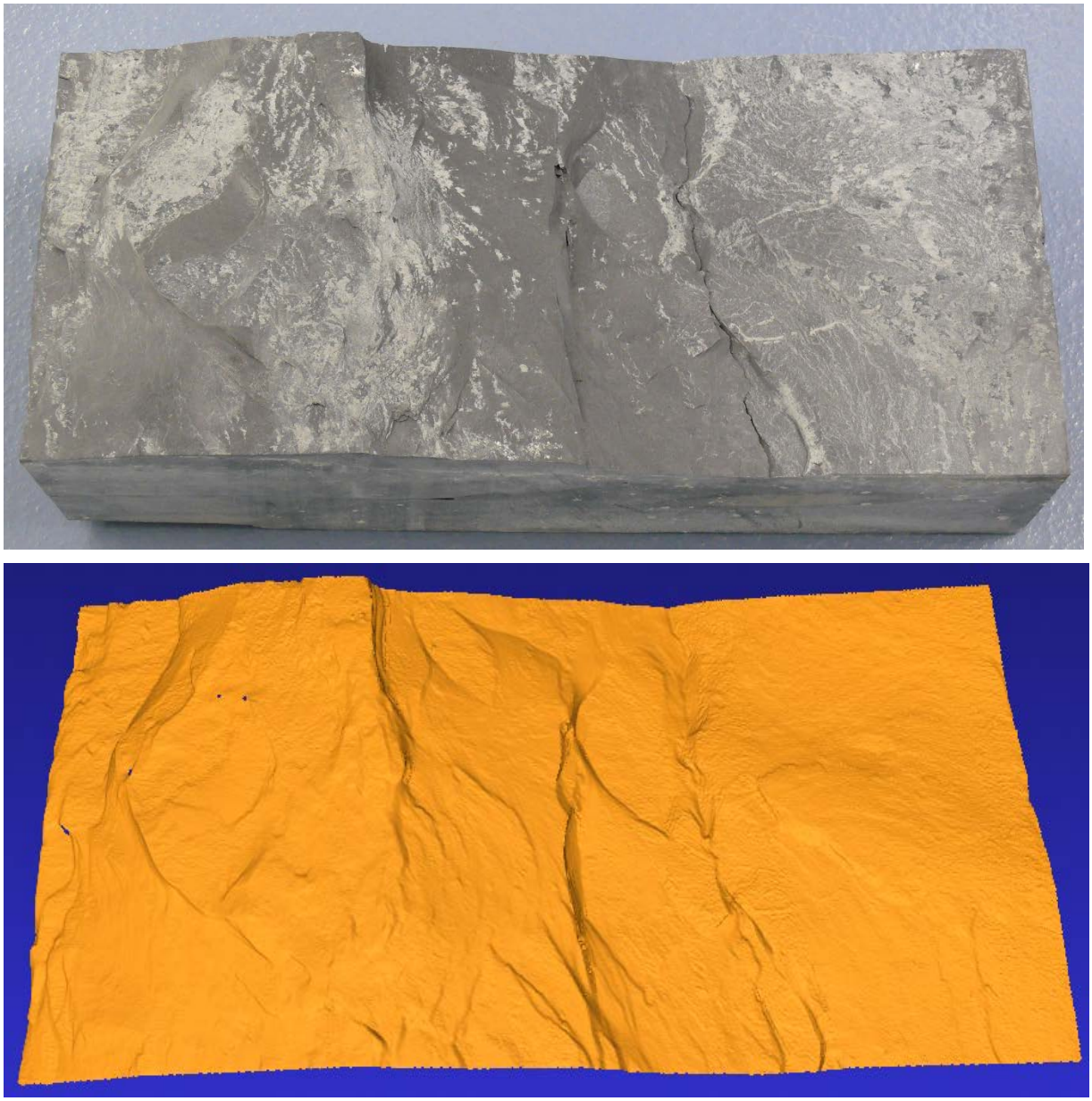

Fig. 21: Surface photo of slate sample (above) and corresponding scanning result (below) (RML 2016)

8 Optical high precision point and profile measurements

High precision 2D optical multi-point and profile measurements can be performed by special optical collimated light systems like the TM-3000 series produced by Keyence (fig. 22). Measurements with this system are based on the 2D image projected on the CMOS receiver. This allows measurements at desired points or measurements with position correction, which is only possible with a 2D device. Accuracy is about 2 µm and up to 16 points can be measured simultaneously. The optical system using a Green LED, and telecentric lenses apply uniform LED light onto the target. This light projects an image on the 2D CMOS and the edges between the light and dark areas are detected to allow measurement at multiple points. Dual telecentric lenses ensure that only collimated light is used for imaging. Even though the distance from the object to the lenses change, the size of the image on the CMOS does not change. High speed and high precision are achieved by performing pinpoint extraction and sub-pixel processing on just the contour within the specified measurement area, from the silhouette imaged on the CMOS. Collimated light is produced without any unevenness by spreading LED light uniformly across the complete range. Examples are shown in figures 23 to 25.

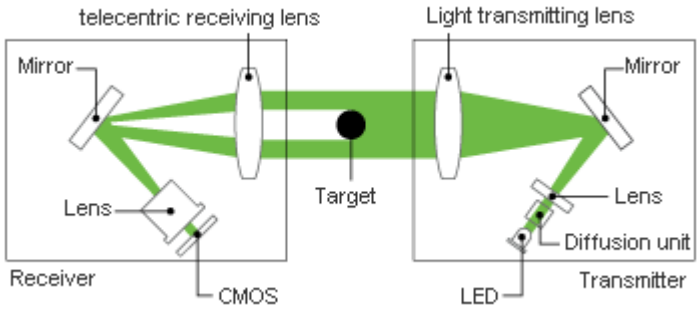

Fig. 22: Principle of optical device TM-3000 (Keyence, company material)

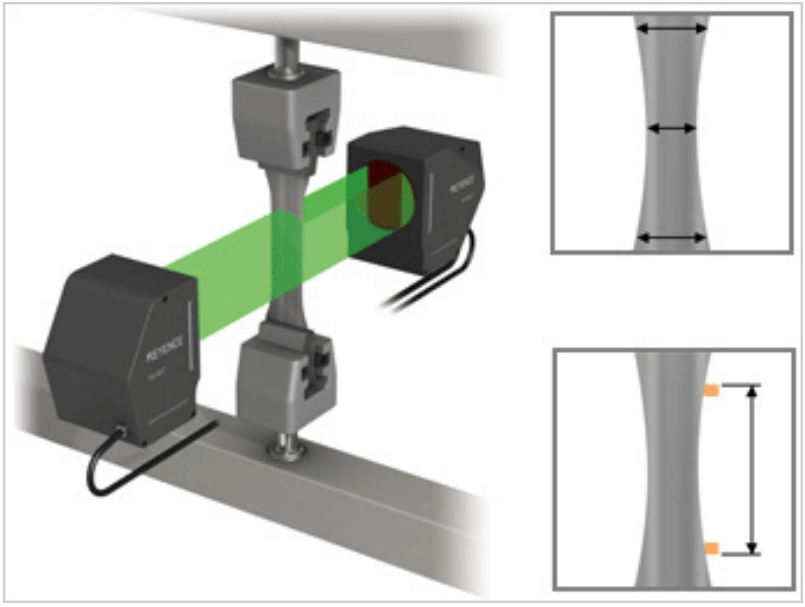

Fig. 23: Thickness measurement of sample during tensile testing (Keyence, company material)

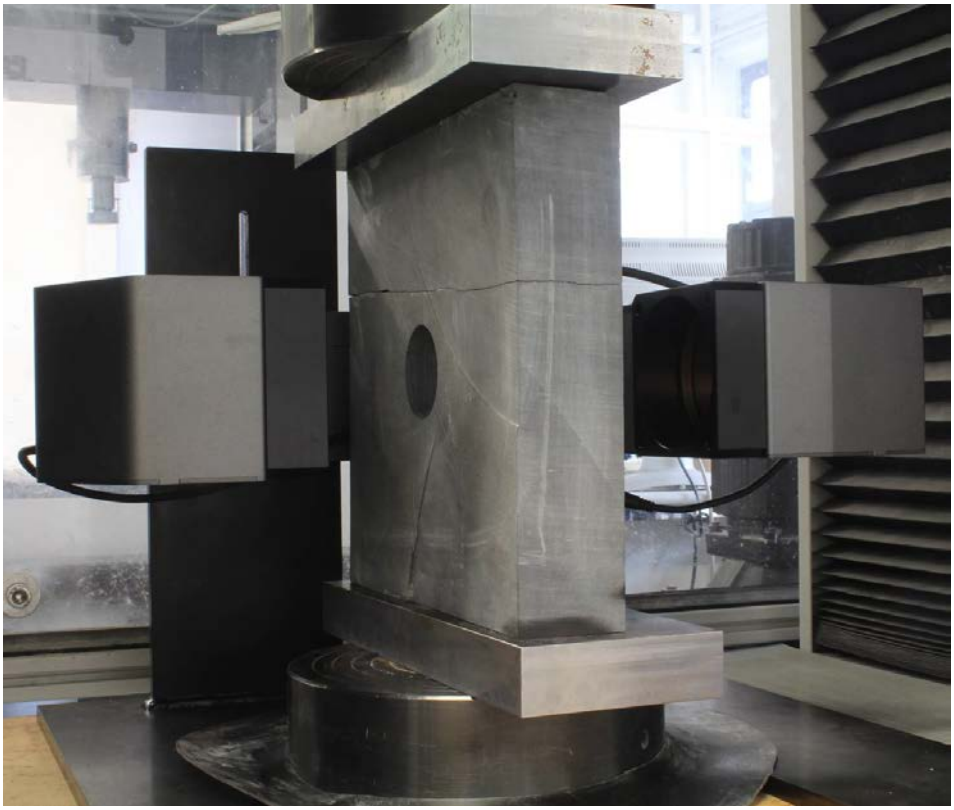

Fig. 24: Monitoring of changes of shape of a circular opening in a rock plate subjected to compressive loading by use of TM-3000 optical measurement device (RML 2016)

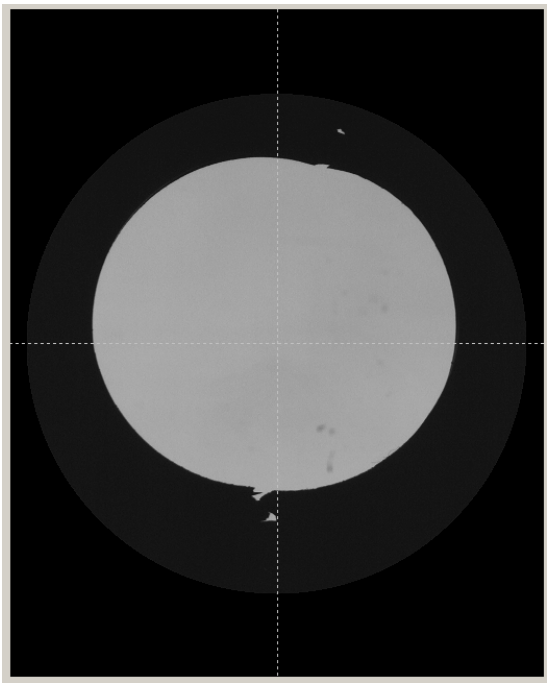

Fig. 25: Detailed view of a circular opening under vertical compressive loading; ovalisation of the opening and tension cracks at top and bottom are shown (RML 2016)

9 Digital Image correlation measurements

Digital Image Correlation (DIC) is a full-field image analysis method, which can determine contours and displacements or deformation velocities of an object under certain loading conditions. It is a non-destructive and non-contact optical technique. DIC can deliver 2D or 3D images. Resolution depends on the field of view (mm^2 to m^2), but can go down to the µm-scale. Typical parameters which can be determined are: actual strain, actual stress, deformation velocities, Young's modulus, Poisson's ratio, crack opening or closure and size of process zone ahead of a crack tip etc.

The working principle (see fig. 26) can be described as follows (company material): "Using a stereoscopic sensor setup each object point is focused on a specific pixel in the image plane of the respective sensor. Knowing the imaging parameter for each sensor (intrinsic parameter) and the orientation of the sensors with respect to each other (extrinsic parameter), the position of each object point in three dimensions can be calculated. Using a stochastic intensity pattern on the object surface, the position of each object point in the two images can be identified by applying a correlation algorithm." A more detailed overview about the DIC technique is provided by Chu and Sutton (1985).

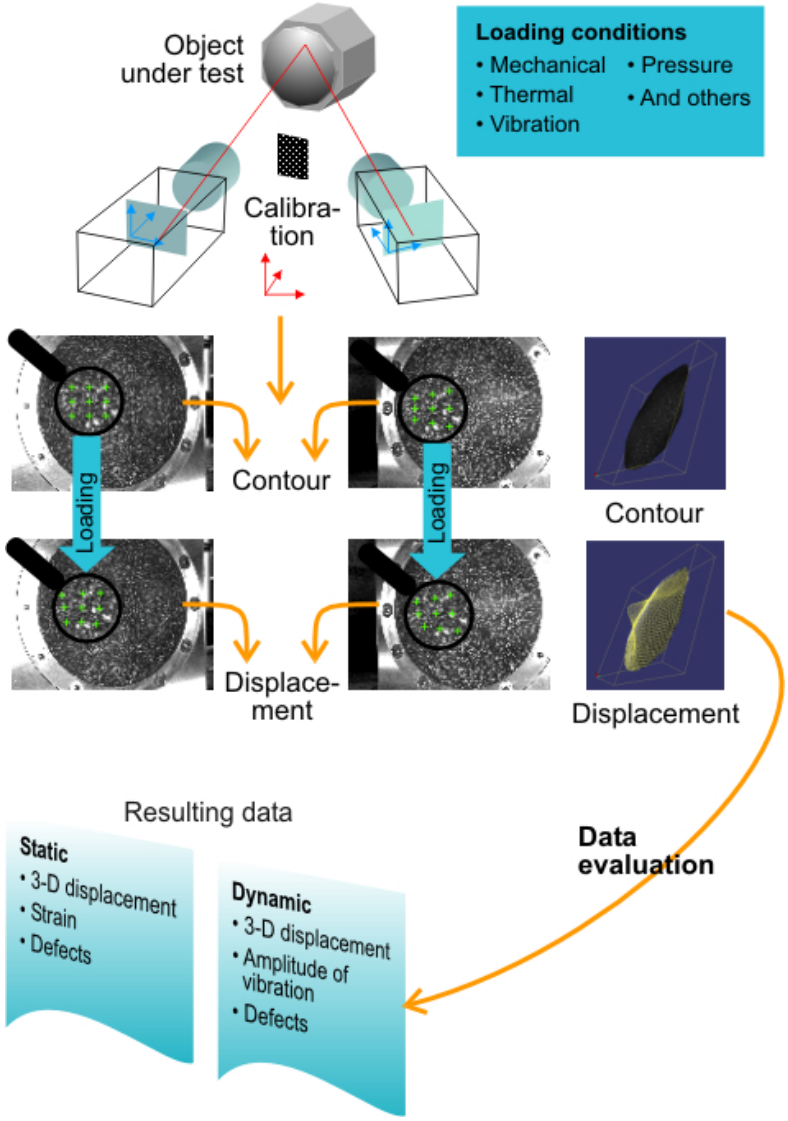

Fig. 26: General set-up of DIC measurement system (company material)

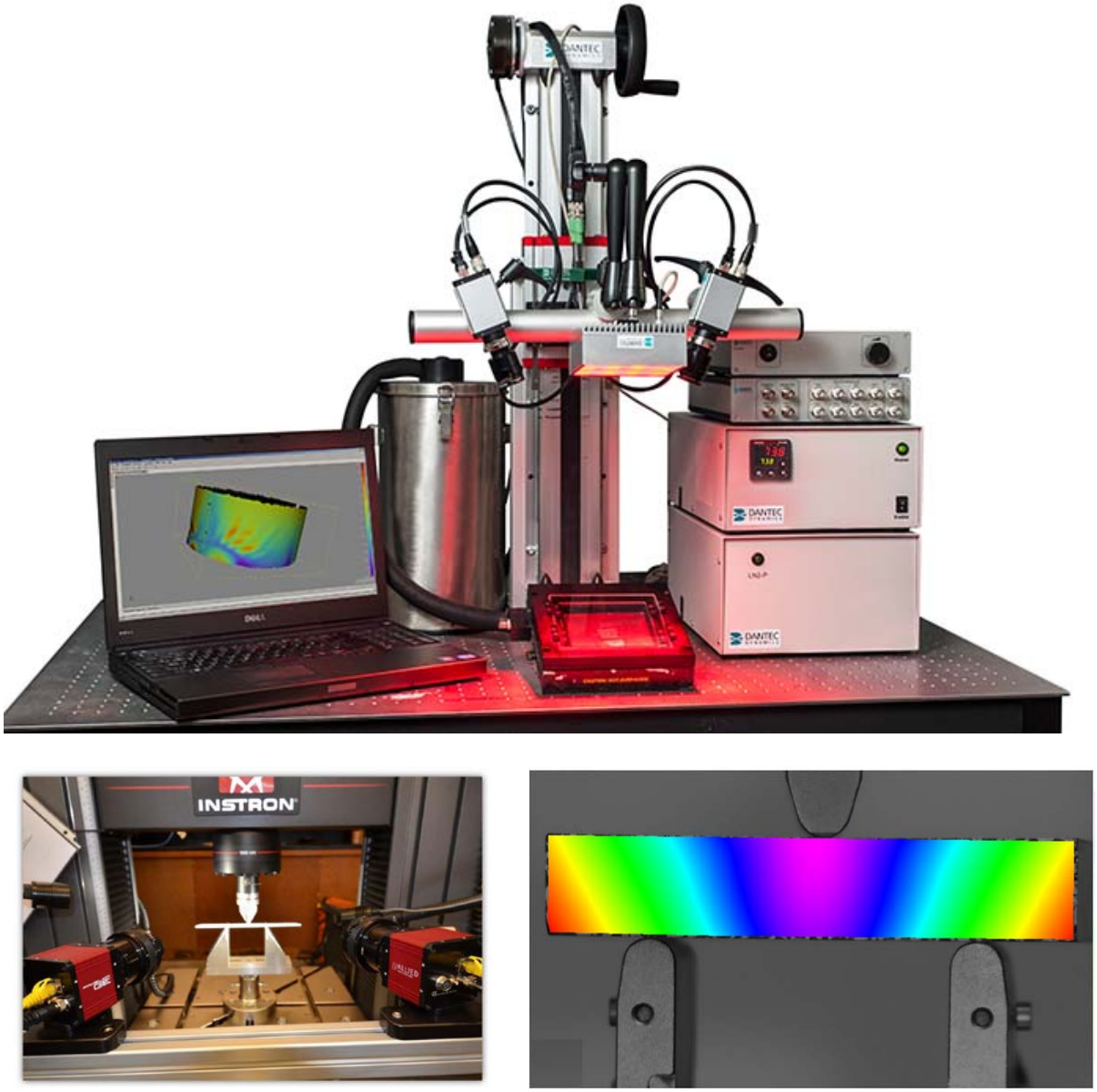

Fig. 27 Exemplary photos or DIC equipment in operation (company material)

Figures 28 to 31 show some selected applications, which document that DIC is able to detect quite small deformations and that local inhomogeneous deformation pattern can be recognised, which is a huge advantage compared to integral measurements like extensometers (LVDT's) or measuring chains.

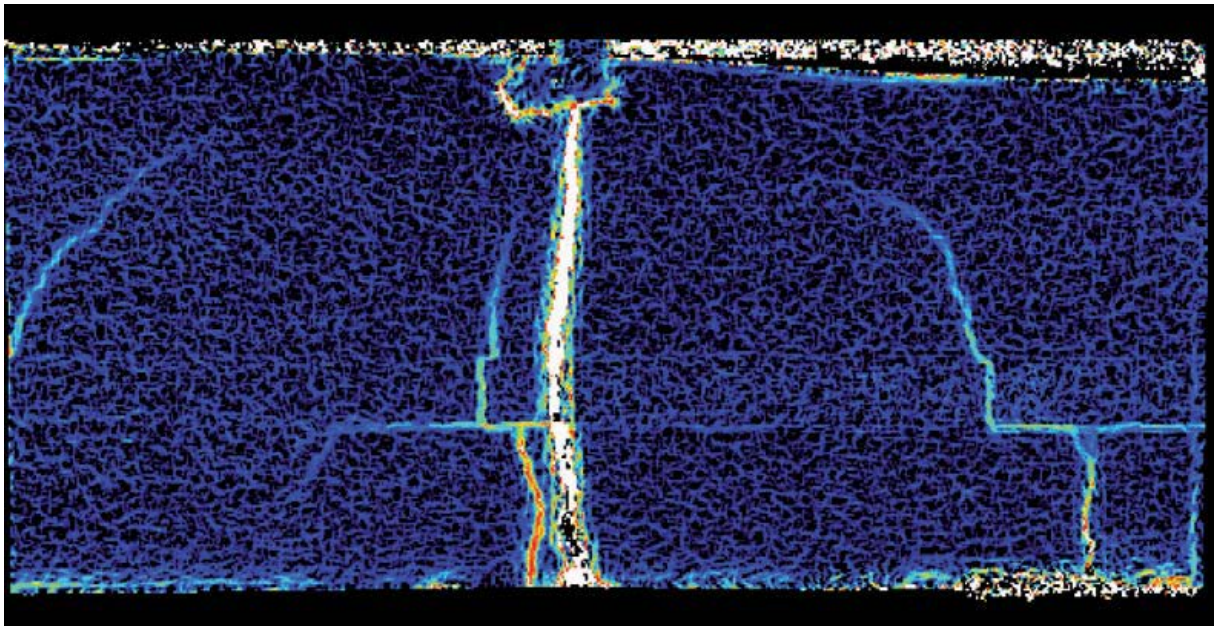

Fig. 28: Detection of microcracks (3-point-bending test) not visible by eyes via DIC (Mc Cormick & Lord, 2010)

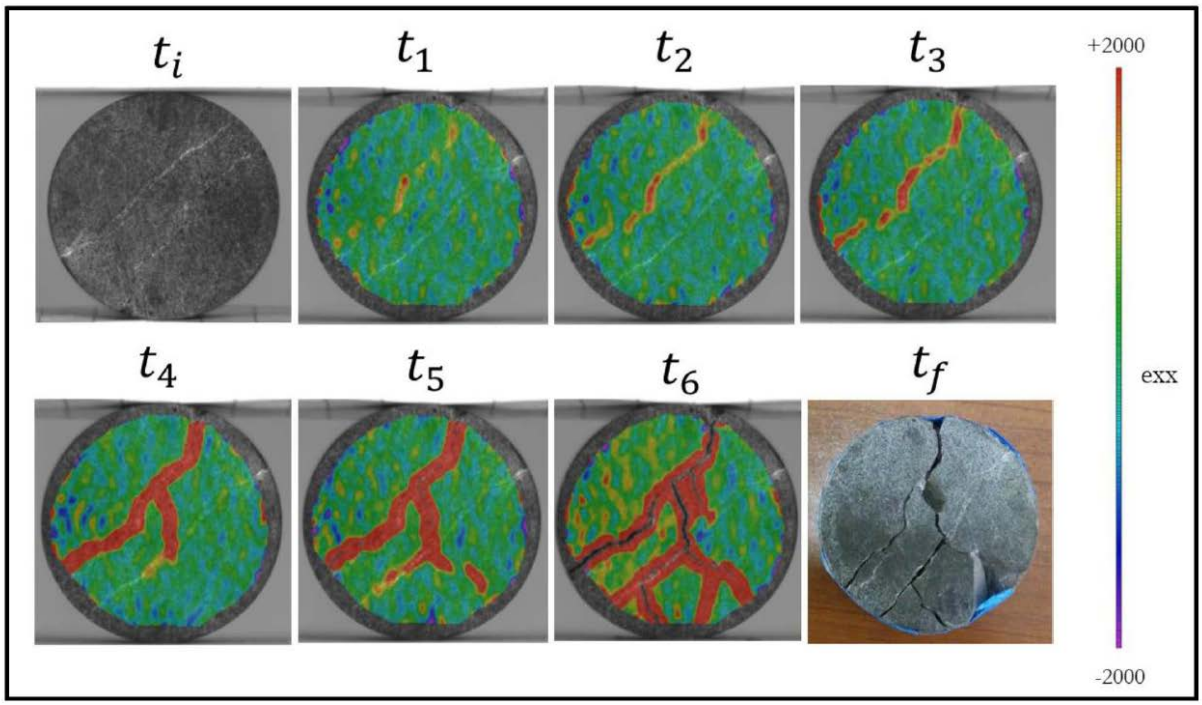

Fig. 29: Strain fields deduced from DIC during Brazilian test of heterogeneous limestone at different points in time (Makhtari et al., 2017)

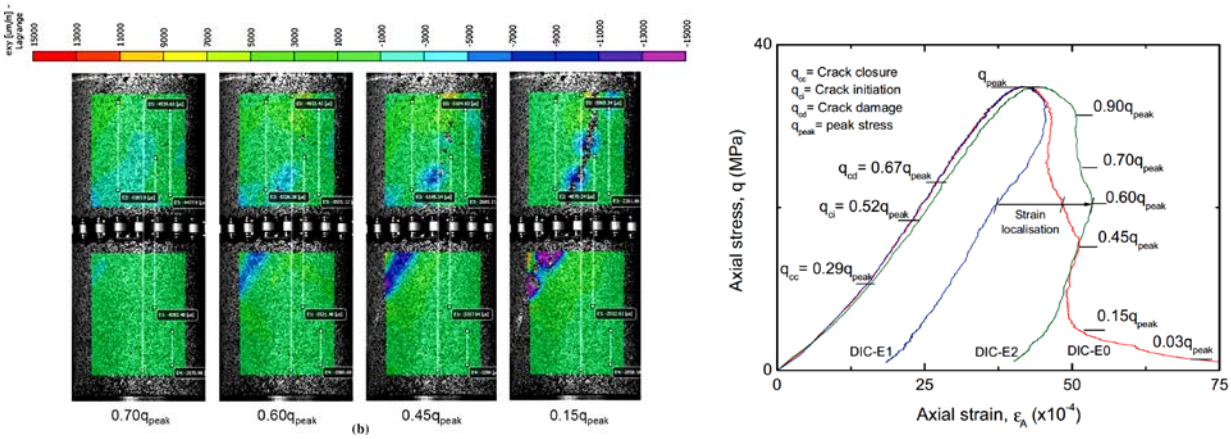

Fig. 30: 3D deformation field (left) and stress-strain relations for virtual extensometers (right) for an uniaxial compression test, both deduced via DIC (Munos, Teheri & Chanda, 2016)

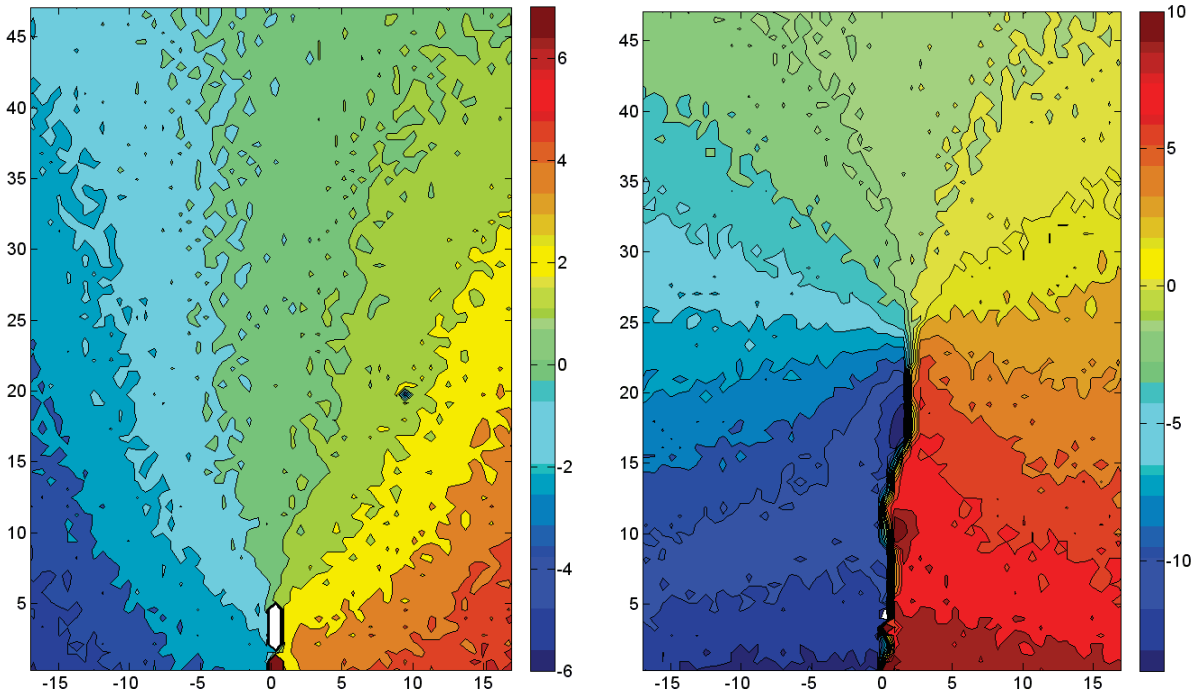

Fig. 31: Mode-I fracture experiment: development of tensile crack starting from a notch. Left: displacement field in the pre-failure region at about 50 % of peak load; right: displacement field in the post-failure region at about 90 % of peak load. All monitored via DIC (Lin & Labuz, 2010).

10 Infrared thermography

Infrared thermography (IRT) is based on thermal radiation from rocks. An image of surface temperature can be obtained. The rate at which energy is emitted depends on the temperature of the rock and its emissivity. The emissivity is the ability of its surface to emit energy by radiation relative to a black body and has a value between 0 and 1 (for rock and concrete this value is greater than 0.9). One also has to consider that measured IR radiation comes from three sources: from the object, from ambient sources and from atmospheric emissions. Infrared radiation covers wave lengths from 0.9 µm to 14 µm. Nowadays sensitivity of IRT cameras can reach app. 0.01 °C and resolution up to 1024 x 1024 pixel. The main parts of an IR camera are illustrated in fig. 32.

IRT is mainly used to detect 'Hot Spots' (heat sources). Crack tips can be considered as moving heat sources, also joints which experience shear displacement are producing heat due to friction. Use of IRT high-speed cameras allows the monitoring of crack propagation or evolution of plastic zones. Figures 33, 34 and 35 show the thermal effect due to the penetration of a wedge into a rock specimen.

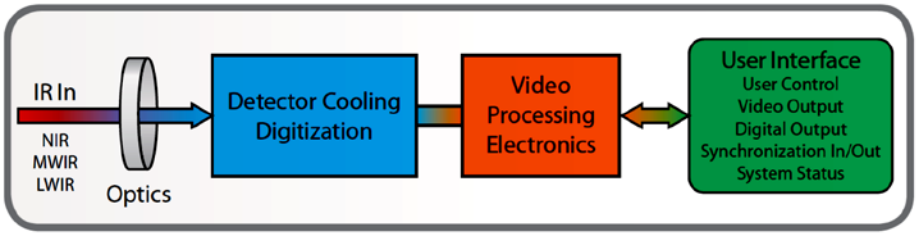

Fig. 32: Simplified block diagram of an IR camera (FLIR: company material)

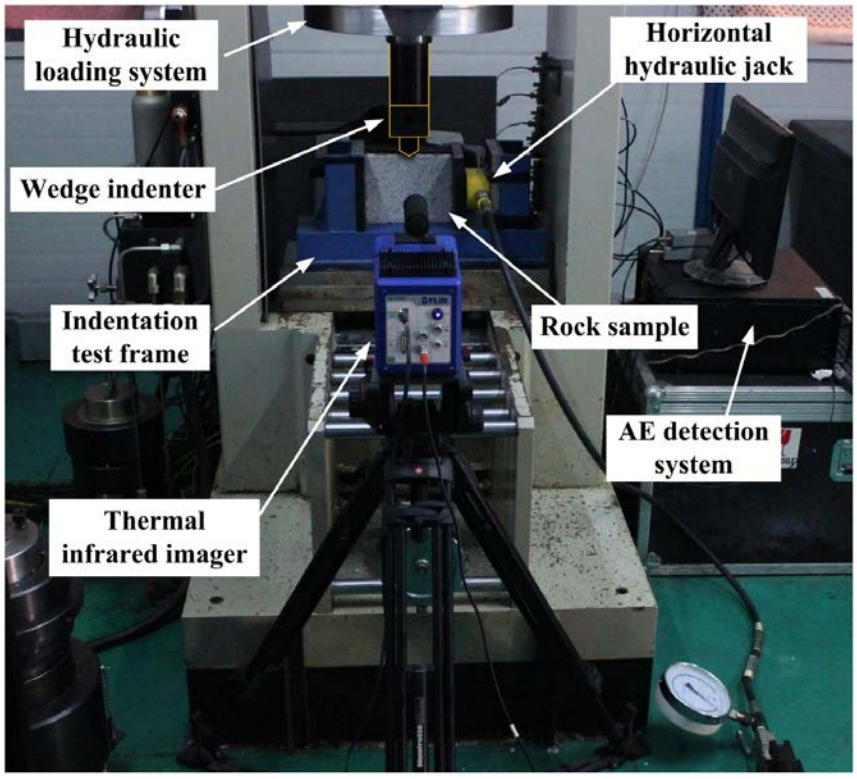

Fig. 33: Test set-up to monitor IR radiation (temperature) and acoustic emission (AE) during wedge penetration test (Liu et al., 2018)

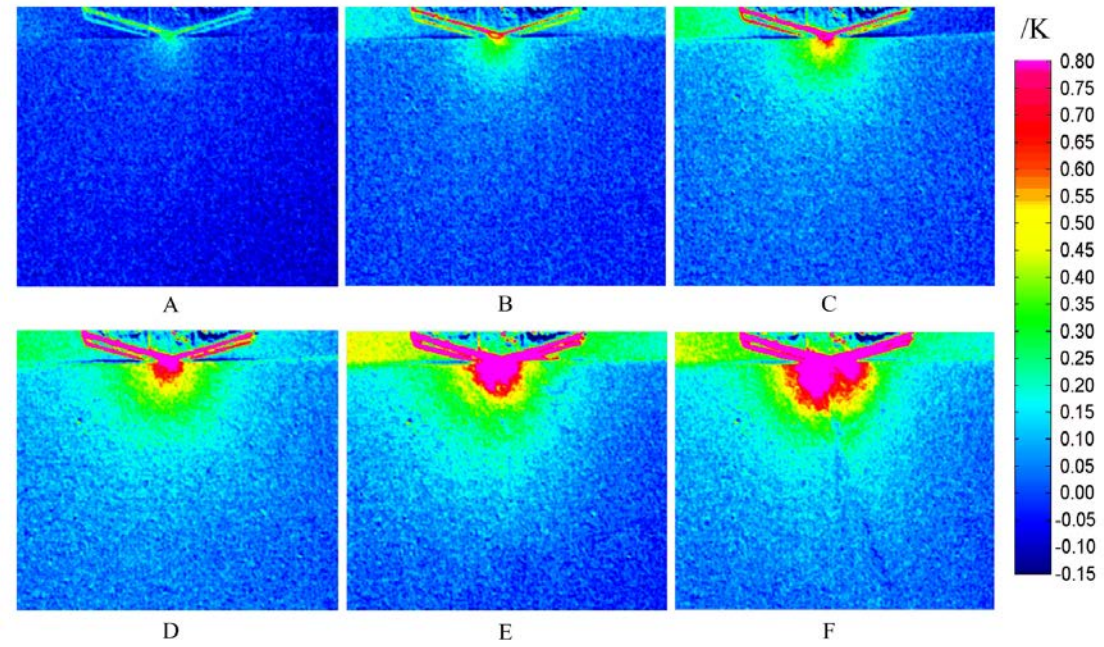

Fig. 34: Temperature change during pushing a wedge into a rock specimen for different time steps (Liu et al., 2018)

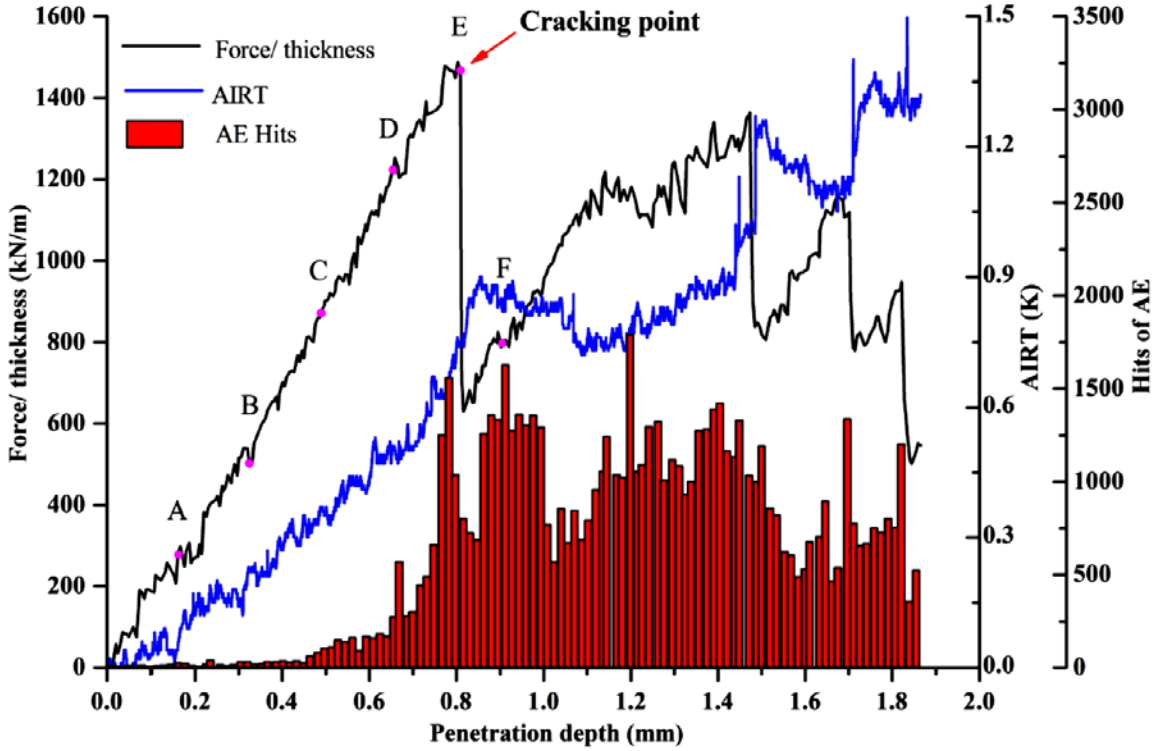

Fig. 35: Development of force, acoustic emission (AE) and temperature change as function of penetration depth of the wedge – see also fig. 27 and 28 (Liu et al., 2018)

11 Positron emission tomography

The method of Positron Emission Tomography (PET) was first developed for and applied in medicin. PET responds to the emission of radiation caused by positron decay. A positron emitting isotop has to be added to a tracer which propagates through the rock (rock matrix or joint). Based on a nuclear decay law the concentration of the decaying nuclide can be calculated based on the measured activity. This method delivers a spatio-temporal distribution of tracer concentration and allows to visualise the fluid flow (flow path and flow velocity). Special devices reach a resolution of about 1 mm (clinical PE scanners reach only about 3 mm). Due to the high local radioactive dose strict safety regulations have to be followed and special equipment is necessary.

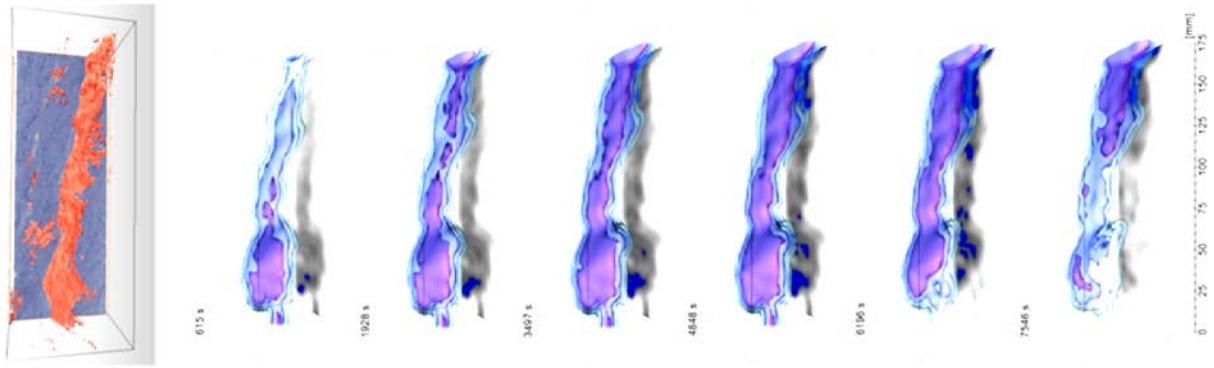

Fig. 36: Fluid flow trough a fracture of a granite sample (diameter: 5 cm, length: 15 cm); Left: µ-CT image of fracture; Other figures: propagation of tracer (Kuhlenkampff et al., 2016)

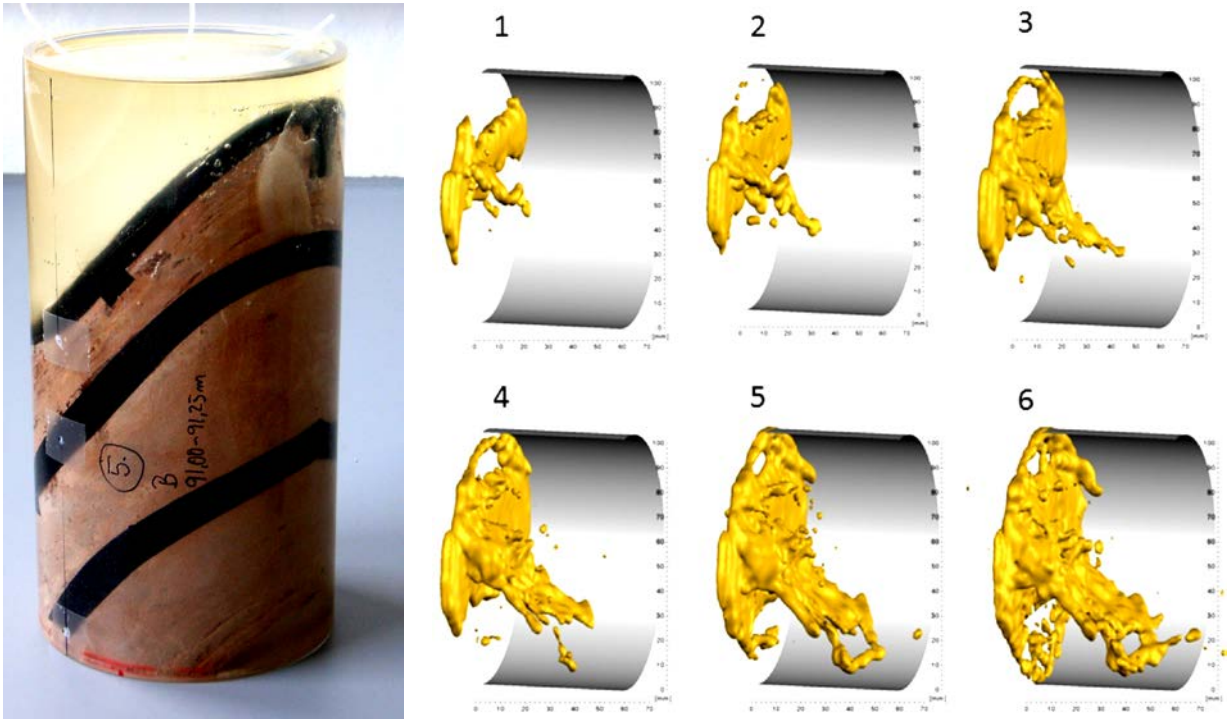

Fig. 37: Fluid flow visualisation through an inclined fracture system in a sandstone sample with a diameter of 10 cm (Kuhlenkampff et al., 2016)

12 Nuclear Magnetic Resonance (NMR)

NMR technology is applied either as logging tool or for lab testing. NMR is mainly used to get information about porosity structure, permeability, damage state, identification of hydrocarbons and producibility in petroleum engineering. It is a non-destructive method. Coates et al. (1999) give a comprensive introduction into this method and Guo et al. (2020) provide an up-dated review.

The NMR technique is based on the magnetic resonance effect of atoms with odd numbers of protons and neutrons. Applying a constant magnetic field leads to a polarization in line with the applied magnetic field and a precession with a specific frequency called Larmor frequency. In addition an oscillating magnetic field is applied with specific Lamor frequencies, which creates a resonance effect which is recorded by coils. After switching off the oscillating magnetic field the nuclei returns back to its original state. This relaxation is measured as either longitudinal relaxation (T_1) or transversal relaxation (T_2).

$T_{1,2}$ can be used to determine the pore size distribution (see Fig. 38) because it is related to the surface relaxation, however pore fluid, bulk (pore fluid) and diffusion transverse relaxation time have also influence and should be considered.

If we consider only surface relaxation, the following relation is valid:

$$\frac{1}{T_{1,2}} = R_{1,2}\left(\frac{S}{V}\right)_{pore}$$

where:

R – surface relaxitivity (material constant, dependent on mineral component)
S - pore surface
V - pore volume.

For a single pore the magnetization M has an exponential decay:

$$M(t) = M_0 e^{-R_{1,2}\left(\frac{S}{V}\right)t}$$

Because rocks have a pore size distribution, the received signal can be considered as a superposition of many individual signals. Use of proper surface relaxitiviy allows to deduce the pore size distribution of the rock as shown in Fig. 39.
Fig. 40 shows a comparison between NMR and MICP measurements for two different types of rock in respect to determined pore size distributions.

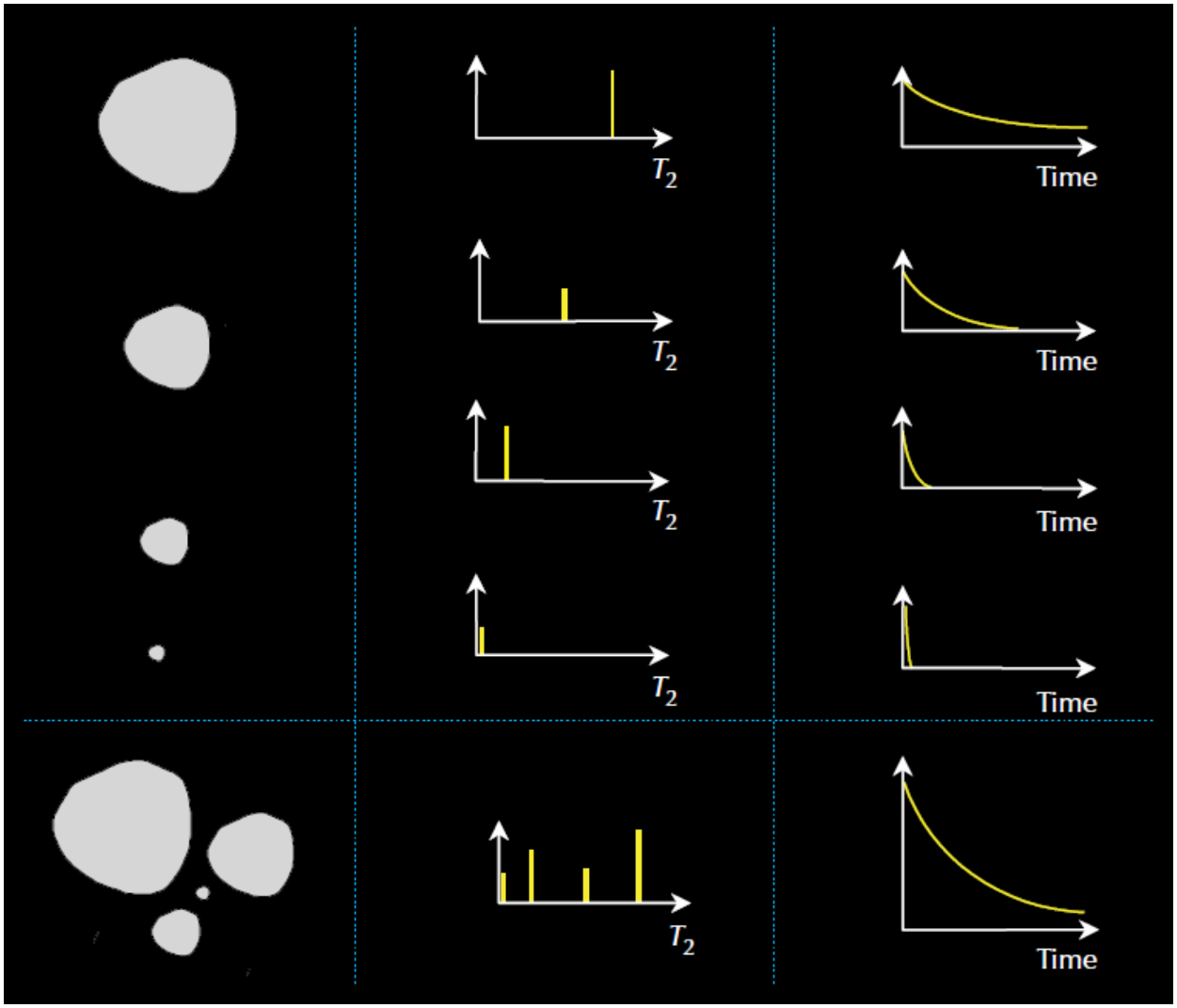

Fig. 38: Illustration of the principal relation bewteen pore size and T_2 (Coates et al. 1999)

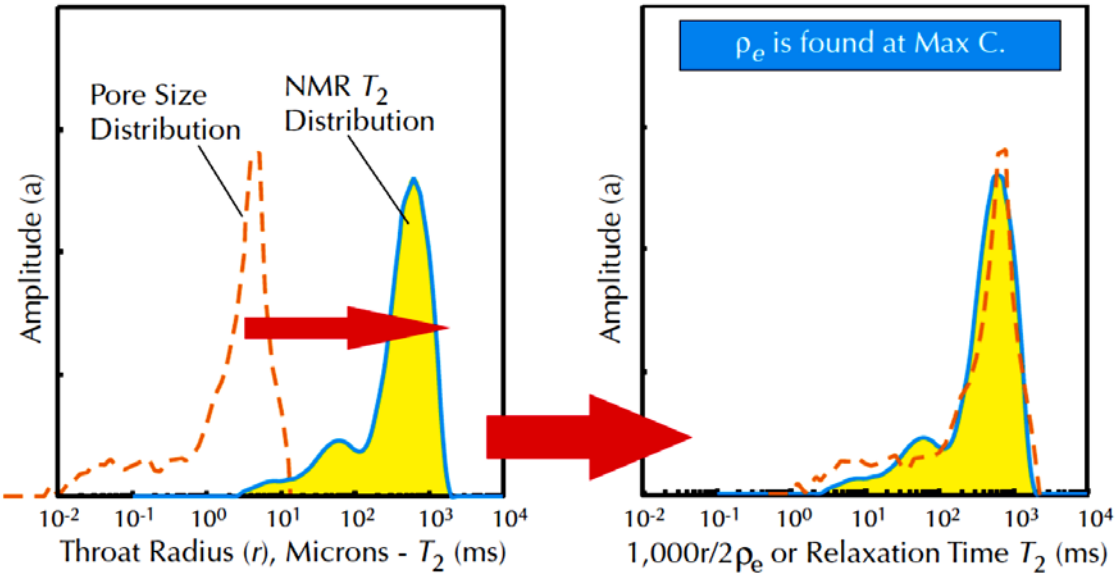

Fig. 39: T_2 distribution vs. pore size distribution (Coates et al. 1999)

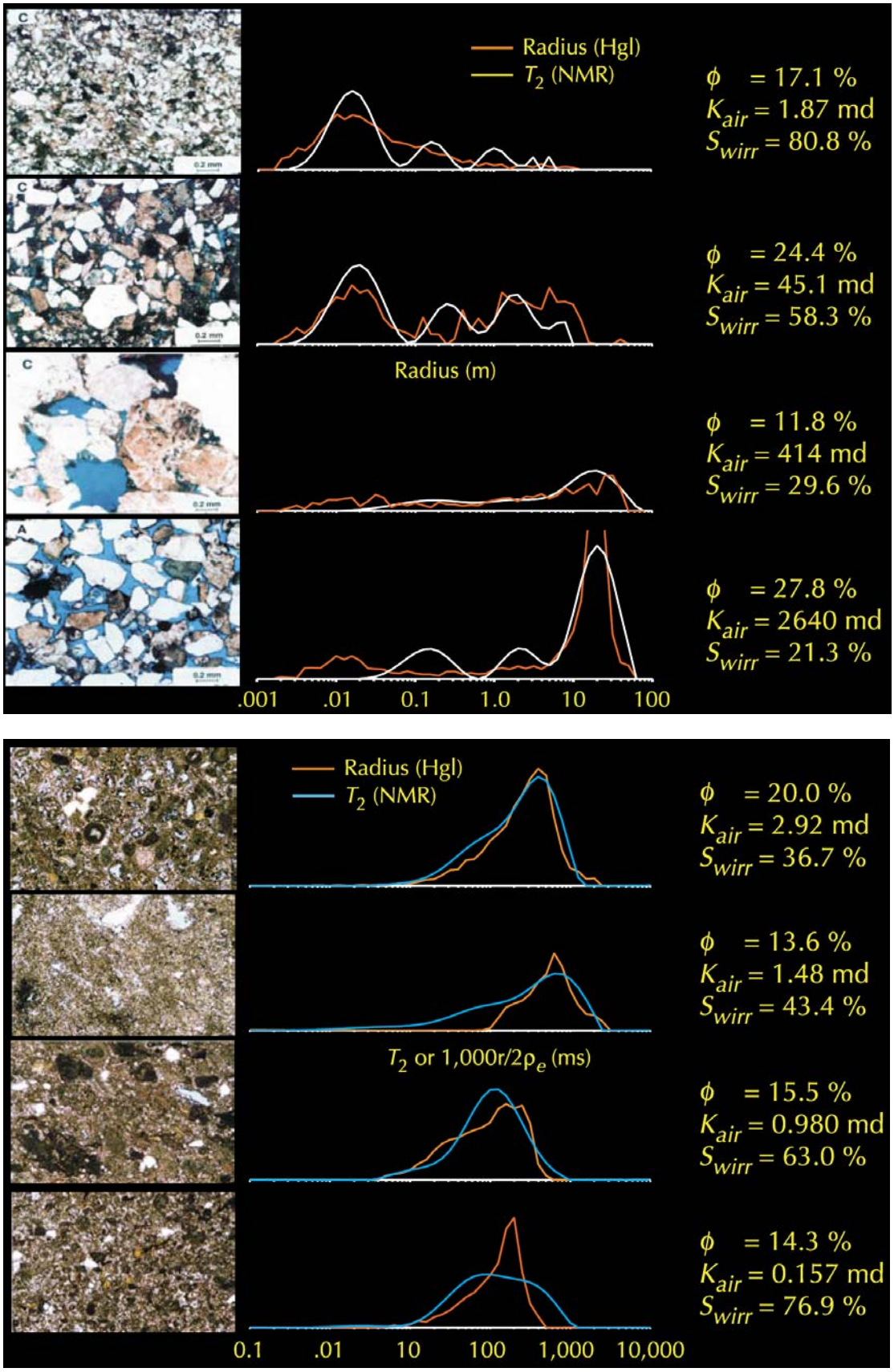

Fig. 40: Pore size distribution determined via NMR and MICP (mercury capillary intrusion pressure measurement), below: carbonatic rock (Coates et al. 1999)

13 Mercury injection capillary pressure (MICP)

The MCIP method (also called MIP = mercury intrusion porosimetry) allows to get several information about the internal structure of the pore network, for instance:

- pore size distribution
- total pore volume
- specific surface area
- free water level determination
- recovery efficiency
- particle size distribution

MICP allows pore size determination from about 2 nm to about 1 mm depending on specification of the instrument. The method uses the non-wetting characteristic of mercury. Please note also, that MICP can only measure the largest entrance into the pores, but not the actual inner volume (see Fig. 41). Giesche (2006) and Jiao et al. (2020) provide a good overview about the assumptions and limitations, but also the potential and evaluation procedures of MICP.

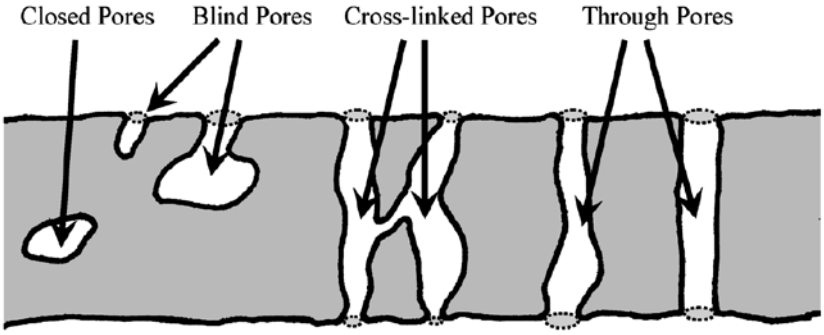

Fig. 41: Sketch to illustrate pore types (Giesche, 2006)

MICP is using a pressure system to inject mercury into the voids of the rock. Pressure is stepwise increased. First, only larger pores all filled. With increasing pressure (up to several 100 MPa) also smaller pores are filled. Inter-particle pores (between the individual particles) as well as intra-particle pores (within the particle itself) can be characterized using this technique.

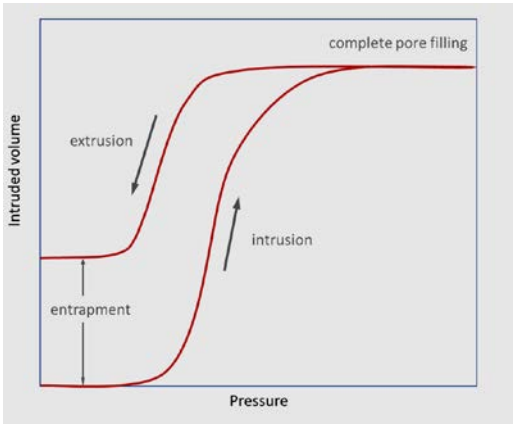

Fig. 42: Idealised pressure – volume curve of a MIP test

Fig. 43: Different MIP devices (company material)

Examplary, Fig. 44 show the MIP based evaluation of several sandstone samples. Permeability, overall porosity and pore size distribution were evaluated.

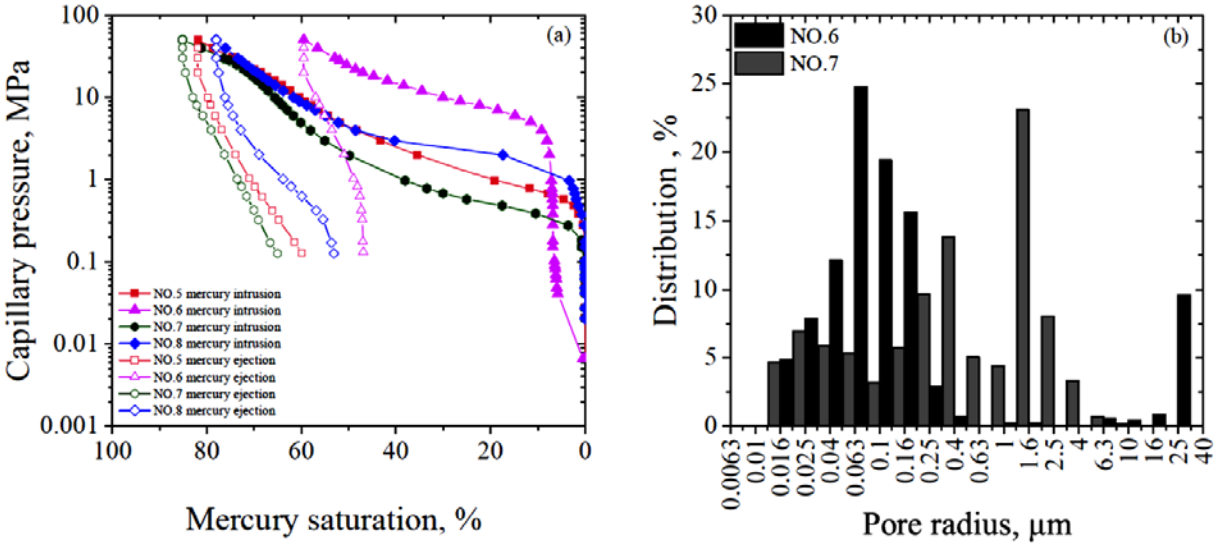

Fig. 44: MIP applied on sandstone samples (Jiao et al., 2020): sample no.6: porosity 5.3%, permeability 0.04 mD; sample no.7: porosity 14.1%, permeability 2.2 mD.

14 Photo-elasticity

Photo-elasticity is a traditional technique to visualize the elastic stress field (stress concentrations and distributions, respectively) for solids under loading, already developed in the 19th century. The principal components of a photo-elastic device are shown in Fig. 44. At the analyzer a fringe pattern is produced by the optical interference of light waves, which is proportional to the principal stress difference (equal to maximum shear stress) according to following equation (assuming isotropic material and 2-dimensionality):

$$\Delta = \frac{2\pi t}{\lambda} K \left(\sigma_1 - \sigma_3 \right)$$

where:

Δ	induced retardation
t	thickness of sample
C	photo-elastic coefficient (material constant)
λ	vacuum wave length
σ_1, σ_3	major and minor principal stress

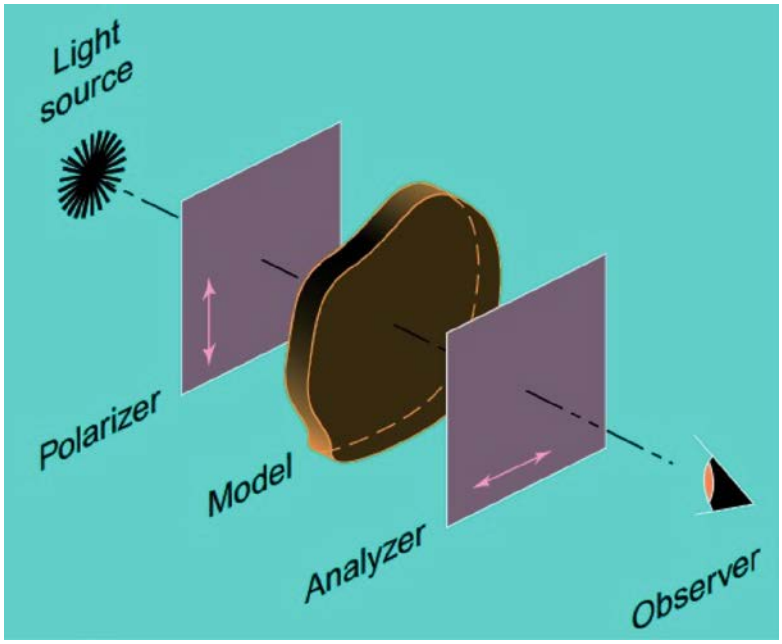

Fig. 45: Principle test set-up of a photo-elastic apparatus (Aydan et al., 2021)

Fig. 46 shows photo-elastic test results for samples under uniaxial loading (plate with two holes; Brazilian test; column with horizontal slot).

Although photo-elasticity is largely replaced by numerical simulation techniques, it has still a cartian significance for the validation of numerical models, for educational purposes due to the fact that stress redistributions due to loading can be observed with naked eyes and for special complex material/shape constellations.

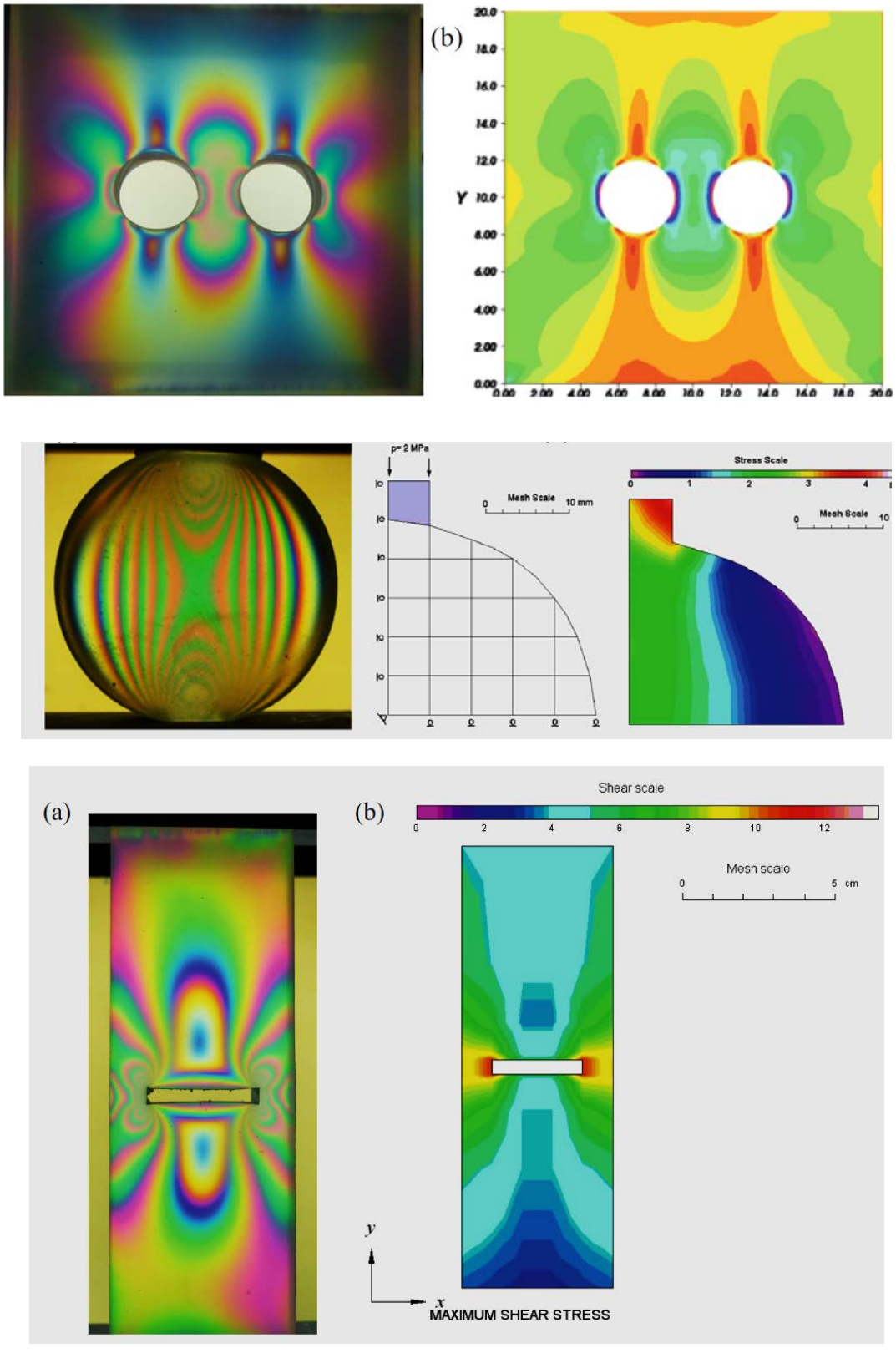

Fig. 46: Examples of fringe pattern and maxium principal stress contours, respectively, obtained by photo-elasticity and FEM simulations (Aydan et al., 2021)

Fig. 47 and 48 show photo-elastic fringe pattern for a sample with complex pore structure.

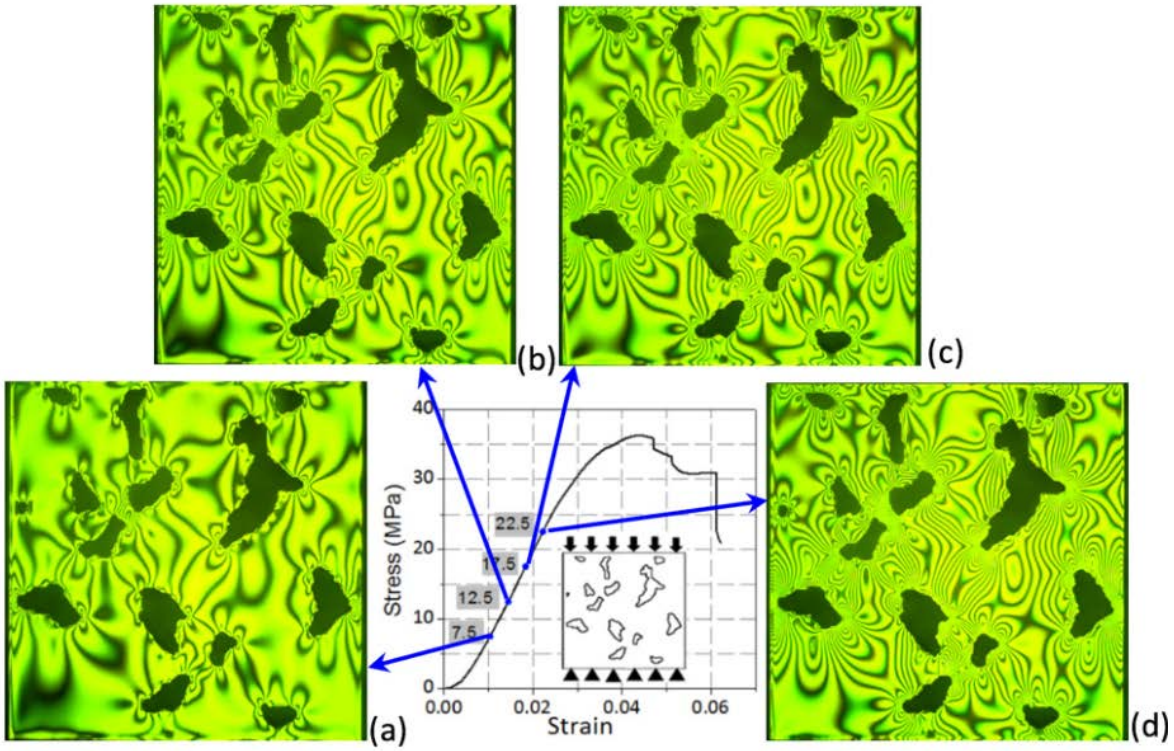

Fig. 47: Fringe pattern of sample with komplex pore structure under uniaxial loading at different stages (Ju et al., 2018)

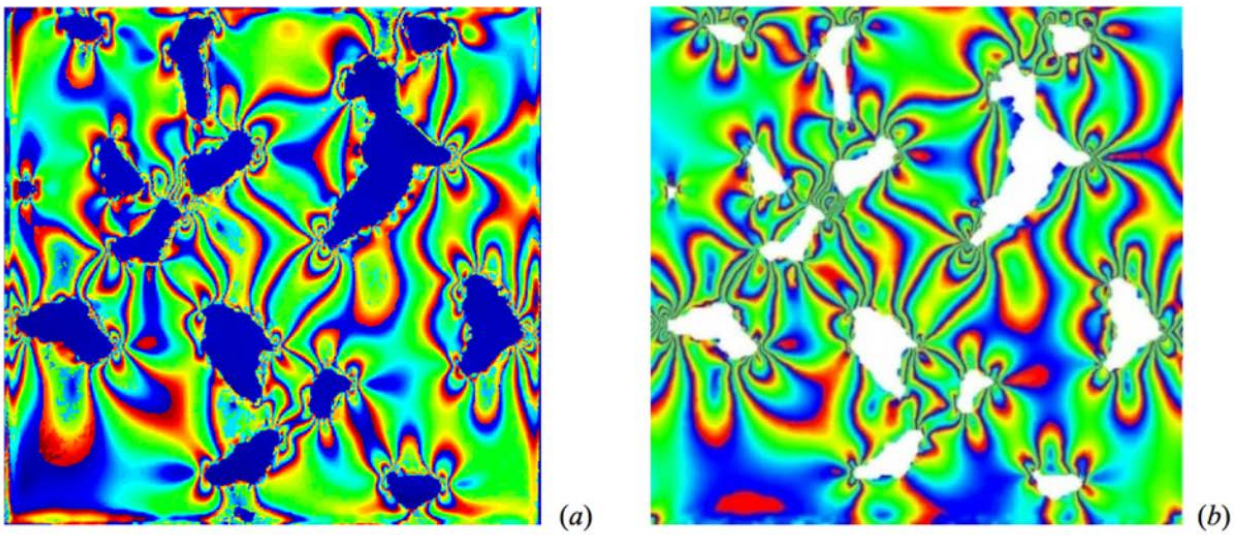

Fig. 48: Fringe pattern (left) and corresponding numerical simulation (right) for sample with complex pore structure under uniaxial loading (Ju et al., 2018)

15 References

Aydan, Ö et al. (2021): A comparitive study on stress distributions in physical models using photo-elasticity and FEM, Proc. IACMAG 2021, Vol. II, 3-11

Baker, D.R., Mancini, L., Polacci, M., Higgins, M.D., Gualda, G.A.R., Hill, R.J. & Rivers, M.L. (2012): An introduction to the application of X-ray microtomography to the three-dimensional study of igneous rocks, *Lithos*, 148: 262-276

Chu, T.P. & Sutton, M. (1985): Applications of digital-image-correlation techniques to experimental mechanics, *Experimental Mechanics*, 232-244

Cnudde, V., Masschaele, B., Dierick, M., Vlassenbroeck, J., Van Hoorebeke, L. & Jacobs, P. (2006): Recent progress in X-ray CT as a geoscience tool, *Applied Geochemistry*, 21(5): 826-832

Coates, G.R. et al. (1999): NMR logging – principles and applications, Halliburton Energy Services, 235 p.

Giesche, H. (2006): Mercury porosimetry: a general practical overview, Part. Part. Syst. Charact., 23: 1-11

Guo, J.-C. (2020): Advances in low-field nuclear magnetic resonance (NMR) technologies applied for characterization of poer space inside rocks: a crticial review, Pteroleum Sciences, 17: 1281-1297

Jiao, L. et al. (2020): Applications of mercury intrusion capillary pressure fo pore structures: a review, Capillarity, 3(4): 62-74

Ju, Y. et al. (2018): Quantitative visualization of the continuous whole-field stress evolution in complex pore structures using photoelastic testing and 3D printing methods, Optics Express, 26(5): 6186

Kaczmarek, L. D.; Zhao, Y.; Konietzky, H.; Wejrzanowski, T.; Maksimczuk, M. (2017): Numerical approach in recognition of selected features of rock structure from hybrid hydrocarbon reservoir samples based on microtomography, In: *Studia Geotechnica et Mechanica*, 39(1): 13-25.

Keyence (2016): Microscope Types and Principles – Main Types of Microscopes, Retrieved from (July 2018): http://www.keyence.com/ss/products/microscope/bz-x700/study/principle/002/index.jsp

Kuhlenkampff, J., Gründig, M., Zakhnini, A. & Lippmann-Pipke, J. (2016): Geoscientific process monitoring with positron emission tomography, *Solid Earth*, 7: 1217-1231

Landis, E.N. & Keane, D.T. (2010): X-ray microtomography, *Materials characterization*, 61(12): 1305-1316

Lin, Q. & Labuz, J.F. (2010): Digital image correlation and the fracture process in rock, *ARMA* 10-431

Liu, Q., Liu, Q., Pan, Y., Peng, X., Deng, P. & Huang, K. (2018): Experimental study on rock indentation using infrared thermography and acoustic emission techniques, *J. Geophys. Eng.*, 15: 1864-1877

McCormick, N. & Lord, J. (2010): Digital Image Correlation, *Materials Today*, 13(12): 52-54

Mokhtari, M., Hayatdavoudi, A., Nizamutdinov, R. & Nath, F. (2017): Characterization of complex fracture propagation in naturally fractured formations using digital image correlation technique, SPE Hydraulic Fracturing Technology Conference and Exhibition, The Woodlands, Texas, USA., SPE-184826-MS

Munos, H., Taheri, A & Chanda, E.K. (2016): Pre-peak and post-peak rock strain characteristics during uniaxial compression by 3D digital image correlation, *Rock Mechanics and Rock Engineering*, 49: 2541-2554

RML (2016): Rock Mechanical Laboratory, Geotechnical Institute, TU Bergakademie Freiberg, Germany

ViALUX (2010), zSnapper Manual, Version 3.0 Rep.

Zhang, Z. et al. (2018): Enhanced poer space analysis by use of µ-CT, MIP, NMR and SIP, Solid Earth, 9: 1225-1238